AFCRL-69-0413

Technical Report 2183-1

THE WIDE ANGLE SIDE LOBES OF REFLECTOR ANTENNAS

P.A.J. Ratnasiri, R.G. Kouyoumjian and P.H. Pathak

The Ohio State University

ElectroScience Laboratory

Department of Electrical Engineering
Columbus, Ohio 43212

Scientific Report No. 4
Contract Number AF19(628)-5929
Project No. 5635
Task No. 563502
Work Unit No. 56350201

23 March 1970

Contract Monitor: John K. Schindler
Microwave Physics Laboratory

This document has been approved for public release and sale; its distribution is unlimited.

Air Force Cambridge Research Laboratories
Office of Aerospace Research
United States Air Force
Bedford, Massachusetts 01730

NOTICES

Qualified requesters may obtain additional copies from the Defense Documentation Center. All others should apply to the Clearinghouse for Federal Scientific and Technical Information.

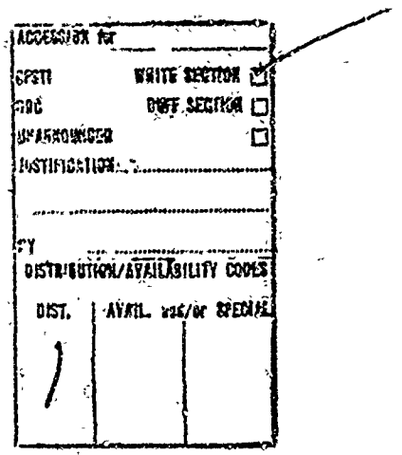

AFCRL-69-0413 Technical Report 2183-1

THE WIDE ANGLE SIDE LOBES OF REFLECTOR ANTENNAS

P.A.J. Ratnasiri, R.G. Kouyoumjian and P.H. Pathak

The Ohio State University
ELECTROSCIENCE LABORATORY
(formerly Antenna Laboratory)
Department of Electrical Engineering
Columbus, Ohio 43212

Scientific Report No. 4
Contract Number AF19(628)-5929
Project No. 5635
Task No. 563502
Work Unit No. 56350201

23 March 1970

Contract Monitor: John K. Schindler
Microwave Physics Laboratory

Air Force Cambridge Research Laboratories
Office of Aerospace Research
United States Air Force
Bedford, Massachusetts 01730

FOREWORD

This report, OSURF Report Number 2183-1, was prepared by The ElectroScience Laboratory, Department of Electrical Engineering, The Ohio State University at Columbus, Ohio. Research was conducted under Contract AF 19(628)-5929. Dr. John K. Schindler, CRDS of the Air Force Cambridge Research Laboratories at Bedford, Massachusetts was the Program Monitor for this research.

ABSTRACT

The geometrical theory of diffraction is applied to calculate the wide angle side lobes of a parabolic reflector antenna. Integral representations are used to correct the field in the forward and rear axial directions. The complete patterns thus obtained are in excellent agreement with experimental patterns when the aperture blockage is not significant. The solution has the usual advantages of a solution based on the geometrical theory of diffraction, namely, it is obtained in the form of simple functions, its computation cost is low, it is directly related to the radiation mechanism of the antenna, and it can be easily modified and extended as the need arises.

CONTENTS

BLANK PAGE

I. INTRODUCTION

This chapter contains a statement of the problem under study and the motivation for undertaking this study, a synopsis of the method of analysis used here, and a brief survey of the previous work on this problem.

A. The Problem

In this report the geometrical theory of diffraction is applied to calculate the wide angle side lobes of reflector antennas. Although there are many types of reflector antennas this discussion will be restricted to rotationally symmetric reflectors. The essential components are shown in Fig. 1; they are the feed antenna and the reflector which serves to form a beam of specified shape. Depending upon the function of the antenna, the reflector surface may be a portion of a paraboloidal, spherical, ellipsoidal or hyperboloidal surface of revolution. However, it is commonly a paraboloid of revolution, and the examples treated here involve a reflector of this type with the feed positioned at the focus.

The calculation of wide angle side lobes including the region behind the reflector has received slight attention, and these side lobes are of practical importance in cases where it is desired to a) reduce the interference between antennas, b) design low noise reflector antennas,[1] c) reduce the radiation hazard to personnel and equipment exposed to high power transmitting antennas.[2]

B. The Approach

The pattern of the reflector antenna is composed of the primary radiation of the feed and the field of the feed diffracted by the reflector. If we consider that the field of the feed is shadowed by the reflector in the geometrical optics sense, the region around the antenna may be divided into an illuminated region and a shadow region where the field is zero. At the shadow boundary the geometrical optics field is discontinuous. In the case of the ellipsoidal and hyperboloidal reflectors there are also far zone reflected fields and associated reflection boundaries.

Employing the geometrical theory of diffraction developed by Keller,[3] the field of the feed induces a class of rays diffracted at the edge of the reflector. These rays radiate into both the illuminated and shadow regions and their fields when properly corrected, as described in App. I, combine with the geometrical optics field to produce a continuous total field at the shadow and reflection boundaries. Rays multiply-diffracted across the aperture are not included in this analysis; most practical reflectors are large enough so that these rays can be neglected.

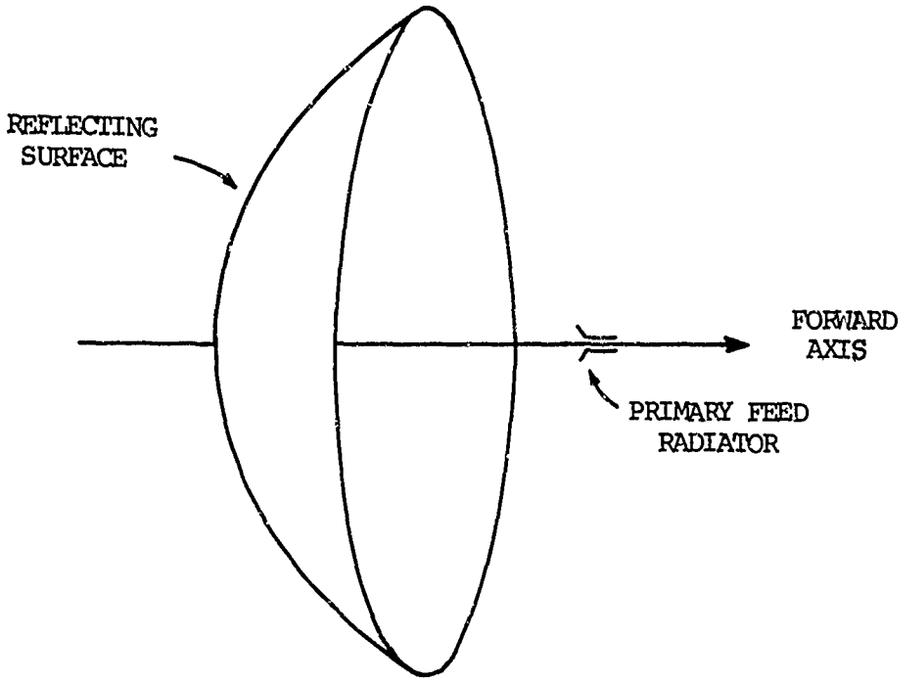

Fig. 1 - Reflector Antenna.

The forward and rear axial directions are caustics of the rays diffracted from the circular edge of the reflector; consequently the geometrical theory of diffraction fails in the neighborhood of these aspects. In the case of the parabolic reflector the forward axial direction is also a caustic of the far zone reflected rays. The fields in the cross-hatched regions of Fig. 2 are calculated from integral representations. In the forward axial region, the conventional aperture field method[4] is employed. In the rear axial direction equivalent electric and magnetic ring currents are employed; these currents are expressed in terms of the edge diffraction coefficients.

In summary, the method of solution described in the following chapters provides a complete 360 degree pattern in any plane containing the antenna axis. Aperture blockage by the feed alone is treated approximately in the usual manner; however, for reasons of simplicity the aperture blockage by the feed support has not been included in the solution.

Although the analysis described in the chapters to follow is applied to calculate the far-zone field of an isolated reflector antenna, it can

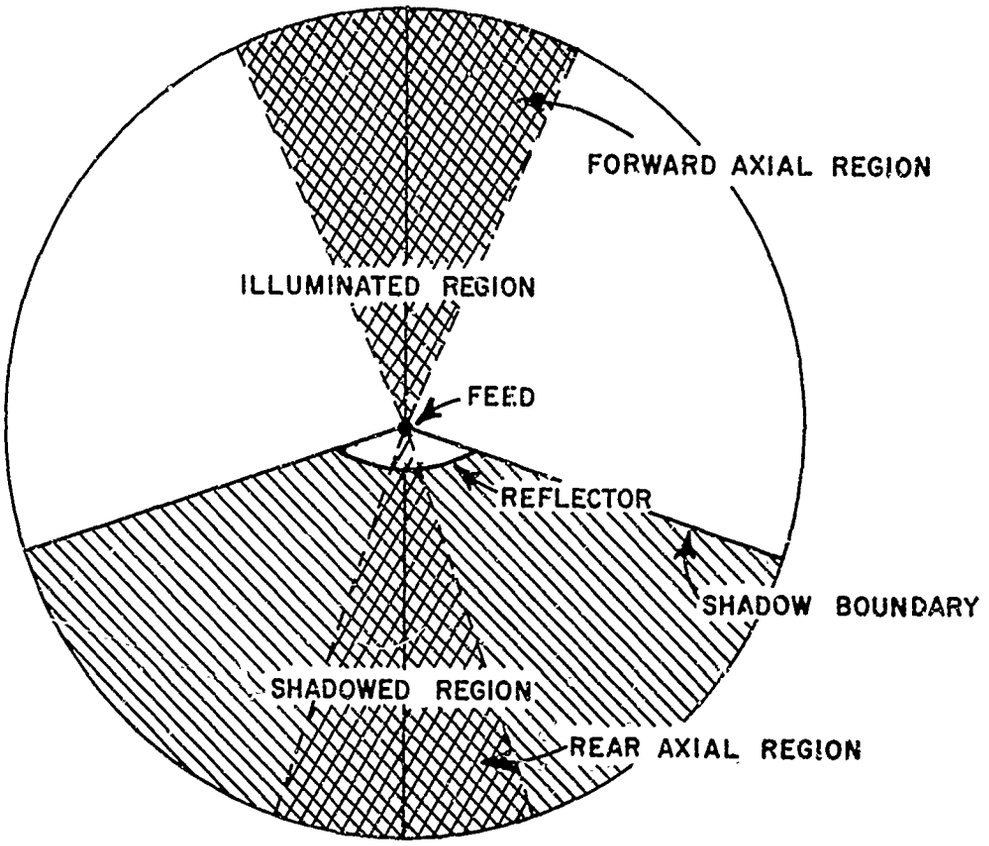

Fig. 2 - Different regions of the secondary field pattern.

be extended to calculate a) the near-zone field, (b) the coupling between reflector antennas, and (c) the environmental effect on the pattern of a reflector antenna.

C. Previous Work

Since the advent of microwaves as a means of tracking and communication, the interest in reflector antennas has grown rapidly. The subject of reflector antennas has been treated extensively by both Silver[5] and Fradin.[6] Though a wide variety of papers on various aspects of this subject have been published, relatively few have been concerned with the wide angle radiation. Tartakovskii[7] studied the radiation pattern of an ideal paraboloid using the current-distribution[8] and aperture-field methods and compared the regions of validity of the two. Schouten and Beukelman[9] applied the current-distribution method to obtain the radiation pattern for a paraboloidal reflector with a dipole feed and expressed

the radiation integral in the form of an infinite series of Bessel functions. Afifi[10] compared the experimental results obtained for the case of a dipole feed with the theoretical results based on the current-distribution method. Computations based on the classical radiation integral are very complicated compared with those based on the geometrical theory of diffraction. Furthermore, they do not correctly predict the pattern behind the reflector.

Kinber[11] was the first to apply the Keller's theory of diffracted rays to this problem. He presented curves which show the general behavior of the pattern for an uniformly illuminated aperture. His results were not corrected for the shadow boundary and the rear axial caustic. Lysher[12] and Peters[13] have both investigated the fields behind a parabolic reflector using the geometrical theory of diffraction, after approximating the real geometry by simplified versions. Lysher approximated the reflector by a flat disc, and Peters considered diffraction at a half plane edge tangent to the edge of the reflector, thereby, neglecting the curvature of the edge. Nevertheless, their results appear to be in reasonable agreement with the measured values. Peters and Rudduck[14] and Peters and Kilcoyne[15] have employed the geometrical theory of diffraction to explain the radiation mechanism of reflector antennas; they also describe how it may be used to improve the design. Recently Rusch[16] studied the edge diffraction for paraboloids and hyperboloids and compared the patterns obtained with those obtained from an integral formula. His results are not valid at the shadow boundary.

In reviewing the previous work it is evident that there is no thorough treatment of the complete pattern of a symmetrical reflector antenna. The previous solutions fail at shadow boundaries or caustics, or else they approximate the reflector geometry.

II. WIDE ANGLE SIDE LOBES

This chapter begins with a description of the physical configuration of the reflector antenna and the various coordinate systems used in its analysis. The field of the primary feed radiation is described next, and subsequently, the two point method to determine the fields away from the axis, and the ring current method to determine the fields in the rear axial region are developed.

A. The Configuration and the Coordinate System

The reflecting surface considered here is a portion of a surface of revolution. Let the vertex of the surface be contained in this portion. A surface of revolution is generated by rotating a curve about a straight line referred to as the axis of revolution. This surface is terminated by a plane perpendicular to the axis; therefore the edge of the surface is a circle and the reflector is said to be axially symmetric. In such a case the circle containing the edge of the reflector is called the aperture circle and the plane containing it, the aperture plane. The paraboloid of revolution and sphere are two reflecting surfaces of widespread practical interest. In the case of the parabolic reflector the shape of the reflector is commonly described in terms of the f/D ratio, i.e. the ratio of the focal length to the diameter.

The reflector is assumed to have a sharp edge and a perfectly conducting surface. The feed is generally placed at the axial focus. Its primary radiation pattern is in general not isotropic. The reflector is assumed to be in the far zone region of the primary radiation field, and the dimensions of the reflector, as well as the distance to the field point are assumed to be large compared with a wavelength, thus the geometrical theory of diffraction can be employed to calculate the field of the edge diffracted rays.

Four coordinate systems are used in this analysis to describe the field of the primary feed, the aperture and edge geometry and the far zone field of the reflector antenna. The field of the feed is described in the spherical coordinate system shown in Fig. 3a, which is centered on the axis of the reflector at the phase reference of the feed; this field may be obtained either from calculation or measurement. The coordinate system shown in Fig. 3b is introduced to describe the field of the feed at the reflector; it has the same origin as the previous coordinate system, but its polar axis is the z axis instead of the y axiz. Setting $\psi = \pi - \theta'$, the transformation of variables and unit vectors, denoted by a superscript, between the two coordinate systems is

$$\cos\psi = \cos\varphi_f \sin\theta_f \tag{1}$$

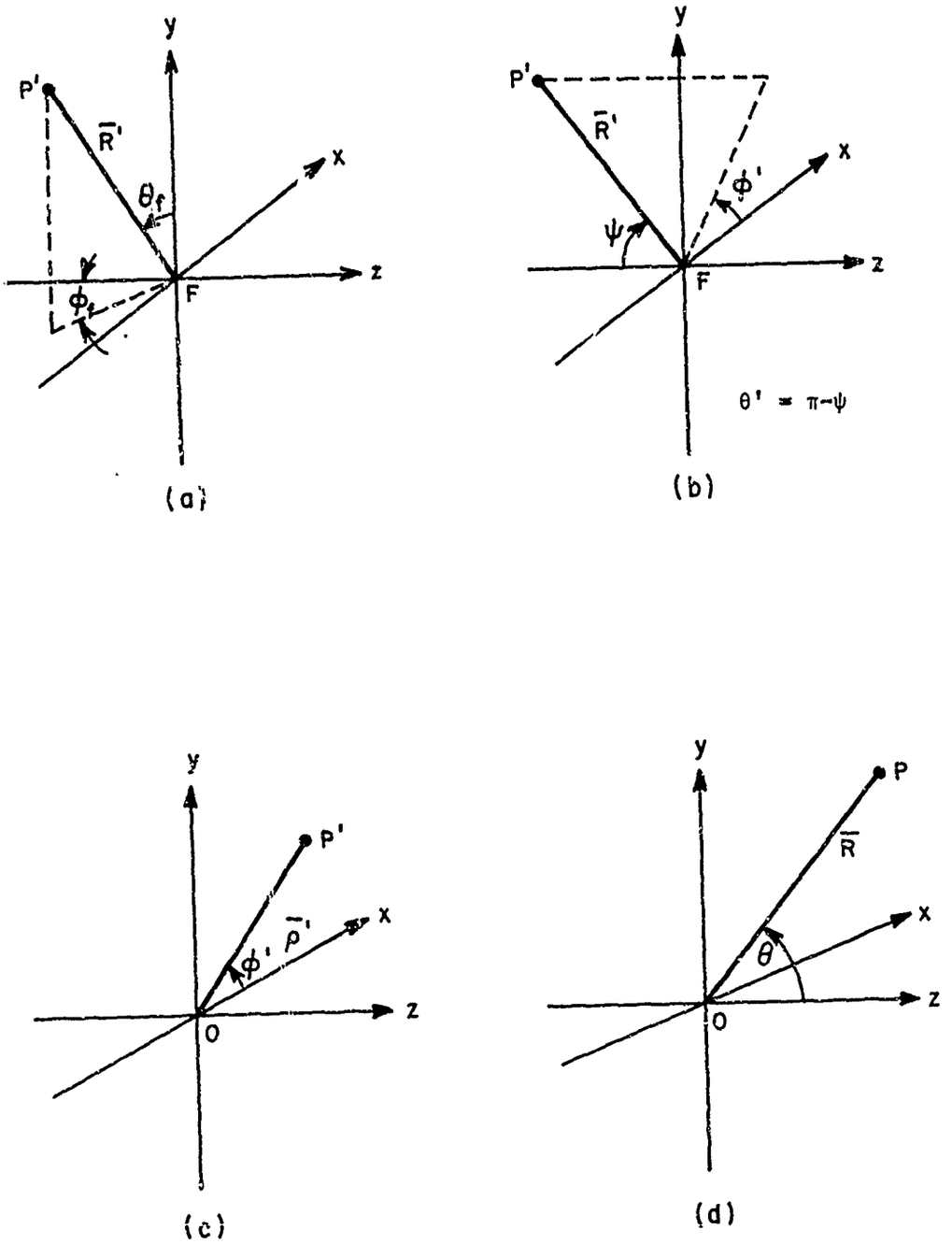

Fig. 3 - Coordinate systems used in the analysis.

(2) $$-\cos\varphi' \sin\psi = \sin\varphi_f \sin\theta_f$$

(3) $$\hat{\psi} = -\hat{\theta}_f \frac{\sin\phi' \cos\psi}{\beta} + \hat{\varphi}_f \left(\frac{\cos\varphi'}{\beta}\right)$$

(4) $$\hat{\varphi}' = -\hat{\theta}_f \frac{\cos\varphi'}{\beta} - \hat{\varphi}_f \frac{\sin\phi' \cos\psi}{\beta}$$

where

(5) $$\beta = \sqrt{1 - \sin^2\psi \sin^2\varphi'} \quad ,$$

The cylindrical coordinate system (ρ',φ',z') shown in Fig. 3c is used to describe the aperture and edge of the reflector; its origin is at the center of the aperture. This coordinate system is useful in the description of the edge diffracted rays, aperture fields, and equivalent edge currents which will be described later. Finally we have the spherical coordinate system shown in Fig. 3d to describe the far zone field of the reflector antenna. The origin of this coordinate system coincides with that of Fig. 3c.

B. The Field of the Feed

For the purpose of the present analysis, the feed is assumed to be a radiator whose dimension is small compared with the aperture diameter and its pattern is assumed to be broadly directional with its maximum value coincident with the reflector axis. Furthermore, for the sake of simplifying the following discussion the pattern of the feed is assured to be linearly-polarized in the direction θ_f. It is clear that this is not an essential restriction because an elliptically polarized field can always be represented as a sum of linearly polarized fields. For the linear polarization state just described the yz-plane is the E-plane and the xz-plane is the H-plane.

In the far zone the field of the feed is given by

(6) $$\bar{E}^f = -\hat{\theta}_f A\, g(\theta_f,\varphi_f) \frac{e^{-jkR'}}{R'} \quad ,$$

where

(7) $$\hat{\theta}_f = -\frac{\hat{R}' \times (\hat{y} \times \hat{R}')}{\sin\theta_f} \quad ,$$

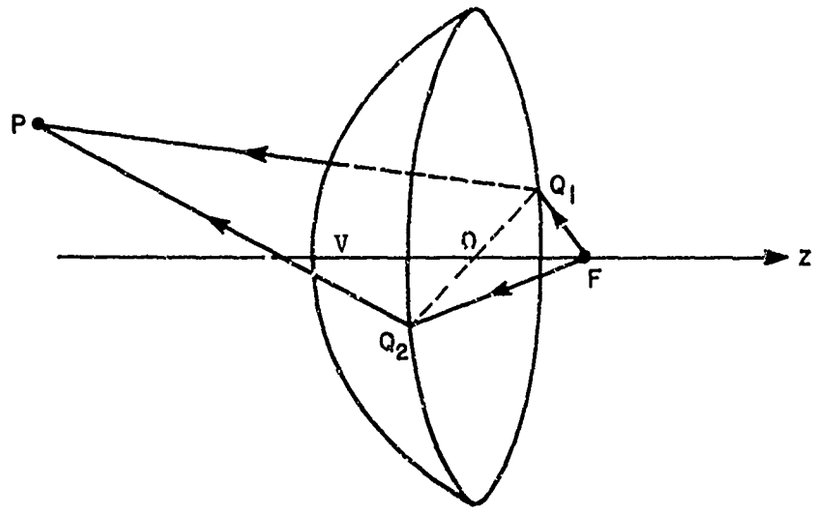

Fig. 4 - The two edge diffracted rays which contribute to the field behind the reflector.

A is the normalization constant,

$g(\theta_f,\varphi_f)$ is the primary feed pattern (with its maximum magnitude equal to unity).

In terms of the coordinate system shown in Fig. 3b

$$(8)\quad \bar{E}^f(R',\psi,\varphi') = -A\left[\hat{e}'\,\frac{\cos\psi\,\sin\varphi'}{\beta} - \hat{\varphi}'\,\frac{\cos\varphi'}{\beta}\right] f(\psi,\varphi')\,\frac{e^{-jkR'}}{R'}\quad ,$$

where

$$(9)\qquad f(\psi,\varphi') = g(\theta_f,\varphi_f)$$

In the E- and H-planes the above expression reduces to

$$(10)\qquad \bar{E}^f_e = \pm\ \hat{\theta}'\,A\,f_e(\psi)\,\frac{e^{-jkR'}}{R'}\quad ,\quad \phi' = \frac{\pi}{2}\quad ,$$

where the sign is determined by $\mathrm{sgn}(-\cos\psi)$.

$$(11) \qquad \overline{E}_h^f = \hat{y}\, A\, f_h(\psi)\, \frac{e^{-jkR'}}{R'} \quad ,$$

in which the pattern functions f_e and f_h may be written as functions of ψ only in the two principal planes.

C. The Two Point Method

As mentioned earlier, this method is used to calculate the field of the reflector antenna at aspects away from the forward and rear axes of symmetry. It should be noted, however, that the two point method is applicable to all practical single reflector antennas.

Earlier it was pointed out that according to geometrical optics concepts the region surrounding the reflector antenna may be divided into an illuminated region and a shadow region. The geometrical optics field at any field point P is then given by

$$(12) \qquad \overline{E}^{g.o.}(P) = \begin{cases} \overline{E}^f(P), & P \text{ in the illuminated region.} \\ 0, & P \text{ in the shadow region.} \end{cases}$$

This geometrical optics field propagates along ray paths which emanate radially from F.

Next let us turn our attention to the diffracted rays and field at P. Consider the path from F to P which also includes a point on the edge of the reflector; the path consists of two straight line sections in a homogeneous medium. There exist two points Q_1 and Q_2 on the edge of the reflector which make the distance along this path a minimum and maximum, respectively. According to Keller's extension of Fermat's principle these minimum and maximum paths are the trajectories of two edge diffracted rays. We may fix Q_1 and Q_2 in the following way. Let V be the vertex of the reflector; the plane defined by FVP intercepts the edge of the reflector at Q_1 and Q_2.

The total field at P

$$(13) \qquad \overline{E}(P) = \overline{E}^{g.o.}(P) + \overline{E}^d(P)$$

where $\overline{E}^d(P)$ is the sum of the fields which are edge diffracted at Q_1 and Q_2. However, over a certain range of θ, the contributions to the diffracted field come only from one of these two points as the other gets shadowed by the reflector itself, as shown in Fig. 5. Thus

$$(14) \qquad \overline{E}^d(P) = \begin{cases} \overline{E}_1^d(P) + \overline{E}_2^d(P), & P \text{ visible from } Q_1 \text{ and } Q_2 \\ \overline{E}_1^d(P), & P \text{ not visible from } Q_2 \end{cases}$$

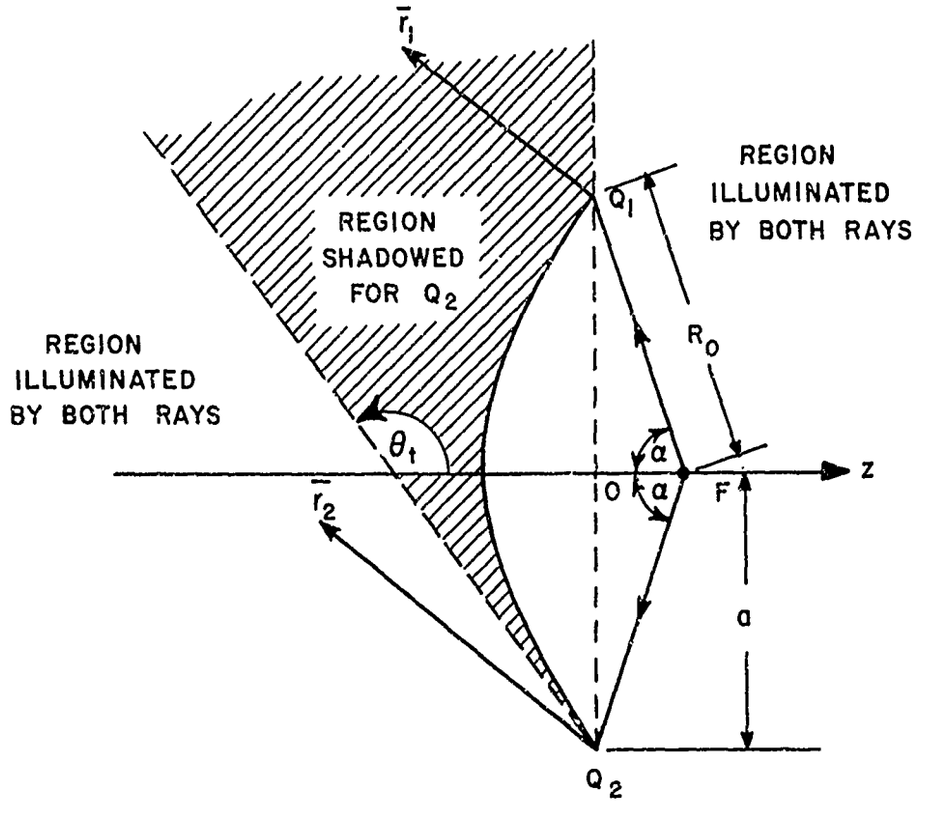

Fig. 5 - Different regions illuminated by the two edge diffracted rays.

where $\bar{E}_1^d(P)$, $\bar{E}_2^d(P)$ are the fields of the edge diffracted rays at Q_1 and Q_2, respectively. The ray incident on the edge at Q_2 gives rise to a surface diffracted ray which propagates along the back surface of the reflector. The surface ray sheds rays tangentially so it propagates into the shadow region shown in Fig. 5. These rays have not been included in our analysis; in general, their effect on the pattern is very small. The contributions from rays multiply-diffracted across the aperture and from rays diffracted from the edge and then reflected from the inner surface of the reflector are small and have been neglected.

Since high frequency diffraction is essentially a local phenomenon, $\bar{E}_i^d(P)$ can be determined in terms of the reflector and ray geometry at the point of diffraction Q_i on the edge. The field of an edge diffracted ray is given by[17]

$$\bar{E}_i^d(P) = \bar{\bar{D}}(Q_i) \cdot \bar{E}^f(Q_i) \sqrt{\frac{\rho_i}{r_i(\rho_i + r_i)}}\, e^{-jkr_i} \quad , \tag{15}$$

where

$\bar{\bar{D}}$ is the dyadic diffraction coefficient for a straight edge,

$\bar{E}^f(Q_i)$ is the electric field of the feed at edge at Q_i, $i = 1, 2$.

ρ_i is the distance of the caustic from the edge at Q_i, and,

r_i is the distance from Q_i to P.

$\bar{\bar{D}}$ and ρ are both as defined by Kouyoumjian,[18] and they are given in App. I and App. II, respectively.

Referring to these appendices, it is seen that $\bar{\bar{D}}$ is a function of the incident and diffracted ray geometries at the edge; it does not depend on edge curvature. The curvature of the edge is taken into account by the divergence factor, the square root term in Eq. (15), which is expressed in terms of the caustic distance at the edge.

Next let us explicitly determine the caustic distance ρ_1, ρ_2 at Q_1, Q_2. We define the radius of the aperture to be a, the distance from the focus F to any point on the edge to be R_o, the angle subtended by the edge at F to be 2α (Fig. 5), the distance from the center of the aperture O to the field point P to be R (Figs. 3d, 4).

As shown in App. II, the caustic distances for this are

$$\rho_1 = \frac{ar_1}{R \sin\theta - a} \quad , \tag{16}$$

and

$$\rho_2 = -\frac{ar_2}{R \sin\theta + a} \quad , \tag{17}$$

Thus at Q_1, the divergence factor becomes

$$\sqrt{\frac{\rho_1}{r_1(\rho_1 + r_1)}} = \frac{1}{\sqrt{r_1}} \sqrt{\frac{a}{R \sin\theta}} \tag{18a}$$

and at Q_2,

(18b) $$\sqrt{\frac{\rho_2}{r_2(\rho_2 + r_2)}} = \frac{j}{\sqrt{r_2}} \sqrt{\frac{a}{R \sin \vartheta}}$$

In the far zone the divergence factors reduce to

(19a,b) $$\frac{1}{R} \sqrt{\frac{a}{\sin \theta}} \quad , \quad \frac{j}{R} \sqrt{\frac{a}{\sin \theta}}$$

at Q_1 and Q_2, respectively. The factor j is caused by the phase discontinuity which occurs at the caustic between Q_2 and the field point.

Substituting from Eqs. (19a) and (19b) into Eq. (15) and making use of the far zone approximations

(20) $$r_1 \simeq R - a \sin \theta \quad ,$$

(21) $$r_2 \simeq R + a \sin \theta \quad ,$$

in the phase term and r_1, $r_2 \simeq R$ in the amplitude, we have for the far zone edge diffracted fields

(22) $$\bar{E}_1^d(P) = \bar{\bar{D}}(Q_1) \cdot \bar{E}^f(Q_2) \sqrt{\frac{a}{\sin \theta}} \frac{e^{-jk(R - a \sin \theta)}}{R} \quad ,$$

(23) $$\bar{E}_2^d(P) = \bar{\bar{D}}(Q_2) \cdot \bar{E}^f(Q_2) \sqrt{\frac{a}{\sin \theta}} \frac{e^{-jk(R + a \sin \theta) + j\frac{\pi}{2}}}{R}$$

It is seen that the scalar product of $\bar{\bar{D}}$ and $\bar{E}^f$ depends on the polarization of the electric field of feed with respect to the diffracting edge. From Eqs. (10) and (11) we see that this electric field is normal to the edge for the E-plane pattern whereas it is parallel to the edge on the H-plane pattern. The pattern in these two planes is of particular interest; the analysis for each case is carried our separately.

a) <u>E-plane Analysis</u> ($\phi = \pi/2$)

The two edge points Q_1 and Q_2 lie in the yz-plane as shown in Fig. 6. Equation (10) yields for the incident field at Q_1,

(24) $$\bar{E}_e^i(Q_1) = (\hat{x} \times \hat{I}_1) A f_e(\alpha) \frac{e^{-jkR_o}}{R_o}$$

in which $\psi = \alpha$ at the edge of the reflector. From Fig. 6 one obtains

$$\hat{e}_1 = - \hat{x} \quad ,$$

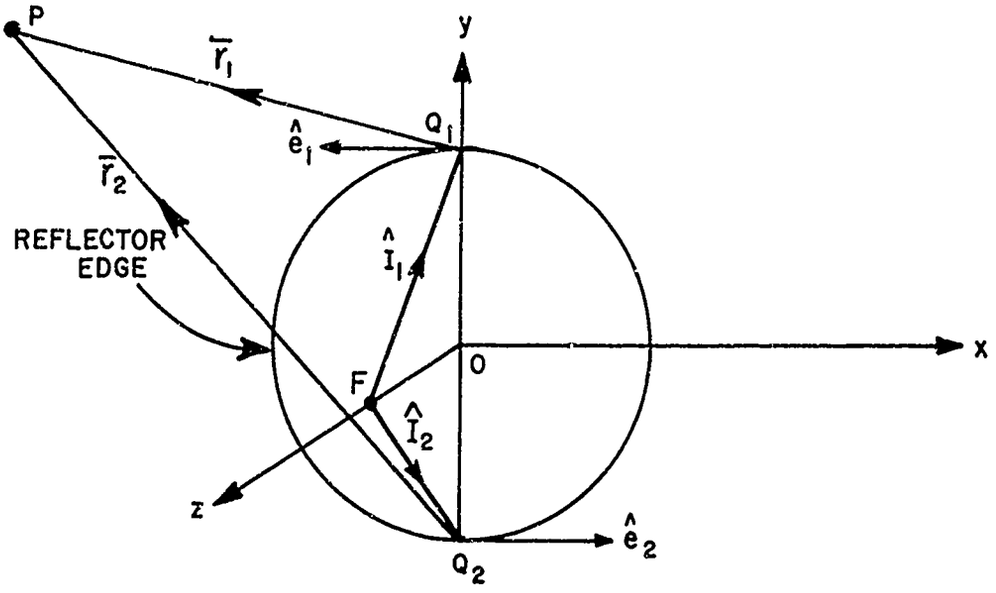

(a) FRONT VIEW

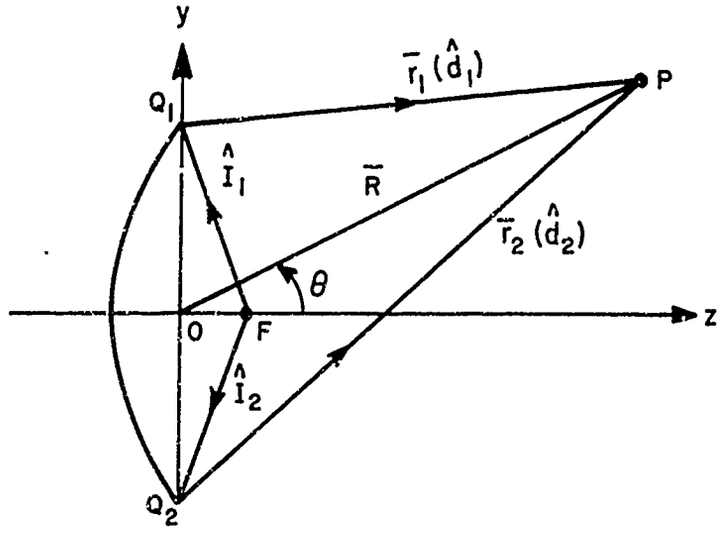

(b) SIDE VIEW

Fig. 6 - Geometry of the edge diffracted rays in the E-plane.

$$\hat{p}_{d_1} = - \hat{x} \times \hat{d} = \hat{\theta}$$

$$\hat{p}' = - \hat{x} \times \hat{I}_1$$

in which we set $\hat{d}_1 = \hat{d}_2 = \hat{d}$ in the far zone. Hence

$$\bar{\bar{D}}(Q_1) \cdot \bar{E}(Q_1) = \left[\hat{x}\hat{x} D_s(Q_1) + (\hat{x} \times \hat{d})(\hat{x} \times \hat{I}_1) D_h(Q_1)\right] \cdot (\hat{x} \times \hat{I}_1) E_e^f(Q_1)$$

$$= - \hat{\theta} D_h(Q_1) A f_e(\alpha) \frac{e^{-jkR_o}}{R_o} \tag{25}$$

Substituting Eq. (25) into Eq. (22),

$$\bar{E}_1^d(P) = - \hat{\theta} A f_e(\alpha) \frac{e^{-jkR_o}}{R_o} D_h(Q_1) \sqrt{\frac{a}{\sin\theta}} \frac{e^{-jk(R - a \sin\theta)}}{R} \tag{26}$$

For the rays diffracted at Q_2,

$$\bar{E}_e^f(Q_2) = (\hat{x} \times \hat{I}_2) A f_e(\alpha) \frac{e^{-jkR_o}}{R_o} \tag{27}$$

and from Fig. 6 one obtains

$$\hat{e}_2 = \hat{x} \ ,$$

$$\hat{p}_{d_2} = \hat{x} \times \hat{d} = - \hat{\theta}$$

$$\hat{p}_2 = \hat{x} \times \hat{I}_2 \ .$$

Following the same procedure as that used for the field diffracted from Q_1, one finds that the field diffracted from Q_2 is

$$\bar{E}_2^d(P) = - \hat{\theta} A f_e(\alpha) \frac{e^{-jkR_o}}{R_o} D_h(Q_2) \sqrt{\frac{a}{\sin\theta}} \frac{e^{-jk(R + a \sin\theta) + j\frac{\pi}{2}}}{R} \tag{28}$$

The field in the E-plane due to the direct radiation from the feed is given by [Eq. (10)]

$$\bar{E}^f(P) = \pm \hat{\theta} A f_e(\psi) \frac{e^{-jkR'}}{R'} \tag{29}$$

which after substituting

$$R' = R - b \cos\theta \tag{30}$$

in the phase term and $R' \simeq R$ in the amplitude reduces to

$$\bar{E}^f(P) = \pm\, \hat{\theta}\, Af_e(\psi)\, \frac{e^{-jk(R - b\cos\theta)}}{R} \quad , \tag{31}$$

where the sign is determined by sgn(cos θ) and

b is the distance between the aperture center and the focus.

b) H-plane Analysis ($\phi = 0$)

The configuration of rays for this case is shown in Fig. 7. The points Q_1 and Q_2 now lie in the xz-plane. The electric field in the incident ray is given by [Eq. (11)]

$$\bar{E}_h^f(Q_1) = \hat{y}\, Af_h(\alpha)\, \frac{e^{-jkR_o}}{R_o} \quad . \tag{32}$$

Therefore

$$\bar{\bar{D}}(Q_1) \cdot \bar{E}^f(Q_1) = [\hat{y}\hat{y} D_s(Q_1) + (\hat{y}x\hat{d})\ (\hat{y}x\hat{I}_1)\ D_h(Q_1)] \cdot \hat{y}\, E_h^f(Q_1)$$

$$= \hat{y}\, D_s(Q_1)\, Af_h(\alpha)\, \frac{e^{-jkR_o}}{R_o} \quad . \tag{33}$$

Next on substituting Eqs. (33) in Eq. (15) and employing Eqs. (19), (20), (21) after making the usual far zone approximations, one obtains

$$\bar{E}_1^d(P) = \hat{y} Af_h(\alpha)\, \frac{e^{-jkR_o}}{R_o} D_s(Q_1) \sqrt{\frac{a}{\sin\theta}}\, \frac{e^{-jk(R - a\sin\theta)}}{R} \quad , \tag{34}$$

$$\bar{E}_2^d(P) = \hat{y} Af_h(\alpha)\, \frac{e^{-jkR_o}}{R_o} D_s(Q_2) \sqrt{\frac{a}{\sin\theta}}\, \frac{e^{-jk(R + a\sin\theta) + j\frac{\pi}{2}}}{R} \quad , \tag{35}$$

and

$$\bar{E}^f(P) = \hat{y} Af_h(\psi)\, \frac{e^{-jk(R - b\cos\theta)}}{R} \tag{36}$$

The total E- and H-plane fields in various regions lying away from the axis can now be obtained on substituting Eqs. (26), (28) and (31) or Eqs. (34), (35) and (36) in Eqs. (13 and 14). If the tangent to the surface at the edge makes an angle θ_t with the z-axis, the region given by $\theta_t < \theta < \frac{\pi}{2}$ will be seen only by one of the two points; see Fig. 5. The shadow boundary for feed illumination is given by $\theta = \pi - \alpha$. The fields contributing to the illumination of the different regions are presented in tabular form; again it is convenient to refer to Fig. 5.

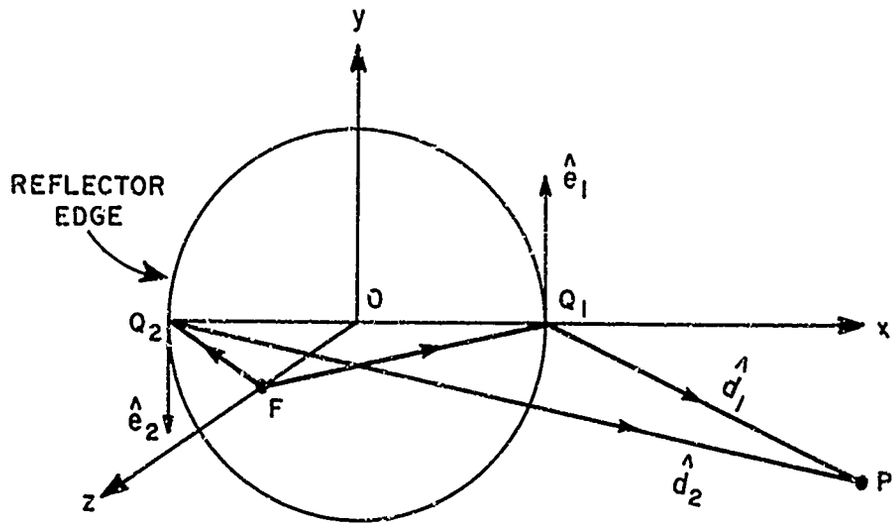

(a) FRONT VIEW

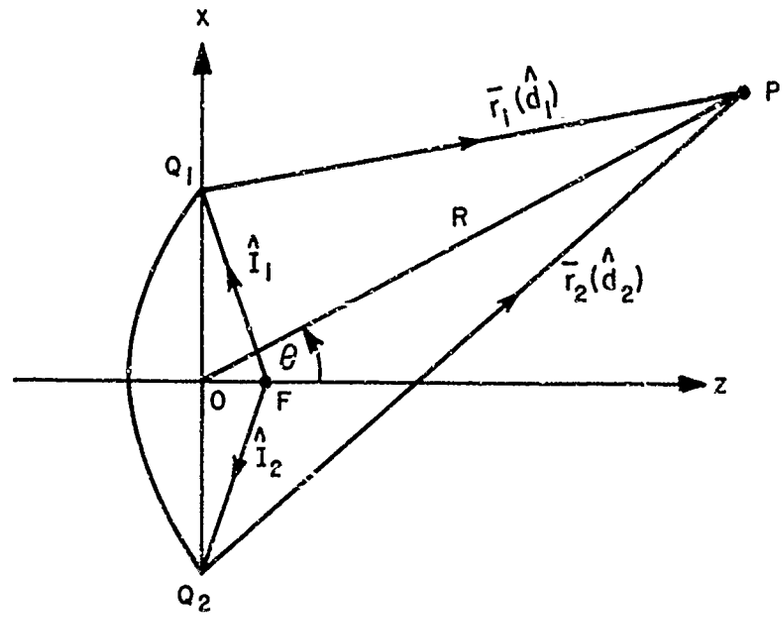

(b) TOP VIEW

Fig. 7 - Geometry of the edge diffracted rays in the H-plane.

Table 1 - Total Fields in Different Regions covered by the Two Point Method

Region	Total Field
$\theta \leq \frac{\pi}{2}$	$\overline{E}^f + \overline{E}_1^d + \overline{E}_2^d$
$\frac{\pi}{2} < \theta < (\pi-\alpha)$	$\overline{E}^f + \overline{E}_1^d$
$(\pi-\alpha) < \theta < \theta_t$	$\overline{E}_1^d$
$\theta_t \leq \theta$	$\overline{E}_1^d + \overline{E}_2^d$

The diffraction coefficients appearing in Eqs. (25) and (33) include the correction factor F which will take into account the smooth variation of the total fields across the shadow boundary. Therefore, this transition region has not been considered separately.

Both the E- and H-plane fields are calculated using this method over the complete range of aspects except in the vicinity of $\theta = 0$ and $\theta = \pi$. The aperture field method and the ring current method will give the contributions to the field at aspects around $\theta = 0$ and $\theta = \pi$, respectively.

D. The Ring Current Method

The rear axis of the reflector forms a caustic for the diffracted rays and therefore, the geometrical theory of diffraction cannot be applied directly to find the field in this direction. As mentioned previously, a different method employing equivalent ring currents will be used for this purpose.

The relationship of these equivalent currents flowing along the edge of the reflector and the scalar diffraction coefficients for the hard and soft boundary conditions may be deduced by examining the two-dimensional diffraction of a plane wave normally incident on a perfectly-conducting half plane. We will consider two cases separately, in one case the incident electric field is parallel to the edge and in the other, the incident magnetic field is parallel to the edge. Using the geometrical theory of diffraction the diffracted electric field in the first case is found to be

$$E^d = E^i(Q)\, D_s(Q) \frac{e^{-jks}}{\sqrt{s}} , \tag{37}$$

and the diffracted magnetic field in the second case to be

(38) $$H^d = H^i(Q)\, D_h(Q) \frac{e^{-jks}}{\sqrt{s}} \quad ,$$

where s is the perpendicular distance from the edge to the field point. Alternatively, these diffracted fields may be described in terms of electric and magnetic line currents I and M flowing along the edge of the half plane.

(39) $$E^d = - kZ_o \frac{e^{j\pi/4}}{\sqrt{8\pi ks}} e^{-jks} I \quad ,$$

and

(40) $$H^d = - kY_o \frac{e^{j\pi/4}}{\sqrt{8\pi ks}} e^{-jks} M \quad .$$

In the case of an arbitrarily polarized incident wave, $E^i(Q)$ must be replaced by its component tangent to the edge $\hat{e} \cdot \overline{E}^i(Q)$ and $H^i(Q)$ must be replaced by its component tangent to the edge $\hat{e} \cdot H^i(Q)$. With this in mind and comparing Eq. (37) with Eq. (39) and Eq. (40), it is seen that the equivalent electric and magnetic edge currents are

(41) $$I = - \frac{\hat{e} \cdot \overline{E}^i(Q)}{Z_o} D_s(Q) \sqrt{\frac{8\pi}{k}} e^{-j\pi/4} \quad ,$$

and

(42) $$M = - \hat{e} \times \hat{I} \cdot \overline{E}^i(Q)\, D_h(Q) \sqrt{\frac{8\pi}{k}} e^{-j\pi/4} \quad ,$$

in which $\hat{I}$ is a unit vector in the direction of incidence and we have made use of the relationship

(43) $$\overline{H}^i(Q) = \frac{\hat{I} \times \overline{E}^i(Q)}{Z_o}$$

It is seen that these equivalent edge currents not only are a function of the position on the edge, but they also depend upon the angles of incidence and diffraction (as defined in Fig. 17 of App. I) at the edge point in question.

These currents are now used to calculate the field directly on the rear axial caustic of the reflector antenna. It can be shown that this procedure leads to a result identical with that obtained when the Braunbek currents[19,20] are employed and the field on the axial caustic is calculated by evaluating the radiation integral asymptotically This latter procedure is known to be a very good high frequency approximation.

At aspects close to the rear axial caustic we employ the same equivalent currents as are used for the rear axial case itself. Strictly speaking this does not seem to be justified, but we find that the patterns calculated by this procedure blend smoothly with the patterns calculated by the two point method. Moreover, we note that near the rear axial caustic D_s and D_h are slowly varying functions of the angle of diffraction in this application, and so keeping them constant for a limited range of aspects is not a poor approximation. These equivalent currents have been used by Ryan[25] to calculate the scattered fields at the axial caustics of several bodies of revolution.

In calculating the field near the rear axial caustic of the reflector

$$I(\varphi') = - \frac{E^f(\varphi')}{Z_o} \cos \varphi' \, D_s \, (\gamma,\gamma') \sqrt{\frac{8\pi}{k}} \, e^{-j\frac{\pi}{4}} \quad , \tag{44}$$

and

$$M(\varphi') = - E^f(\varphi') \sin \varphi' \, D_h \, (\gamma,\gamma') \sqrt{\frac{8\pi}{k}} \, e^{-j\frac{\pi}{4}} \tag{45}$$

where the angles γ,γ' are the angles of diffraction and incidence at the edge of the reflector as shown in Fig. 8. The electric field $\bar{E}^e$ produced by the ring current $I(\varphi')$ is given by the radiation integral (App. III).

$$\bar{E}^e = \frac{jkaZ_o}{4\pi} \frac{e^{-jkR}}{R} \int_0^{2\pi} I(\varphi') e^{jka \sin \theta \cos (\varphi-\varphi')} (\hat{R}x\hat{R}x\hat{\varphi}') \, d\varphi' \tag{46}$$

and the electric field produced by the magnetic ring current $M(\varphi')$ is given by

$$\bar{E}^m = \frac{jka}{4\pi} \frac{e^{-jkR}}{R} \int_0^{2\pi} M(\varphi') e^{jka \sin \theta \cos (\varphi-\varphi')} (\hat{R} \times \hat{\varphi}') \, d\varphi' \quad . \tag{47}$$

The total electric field is then given by the superposition of $\bar{E}^e$ and $\bar{E}^m$. Thus

$$\bar{E} = \bar{E}^e + \bar{E}^m \quad . \tag{48}$$

In order to evaluate these integrals it is necessary to express the field of the feed $\bar{E}^f$ as a function of φ'. $\bar{E}^f(\varphi')$ can be determined from measurement or calculation. In the former case it is customary to measure the E- and H-plane patterns of the feed. The measurement of the feed patterns in these two planes may suffice, if the difference between the two patterns is not too great.

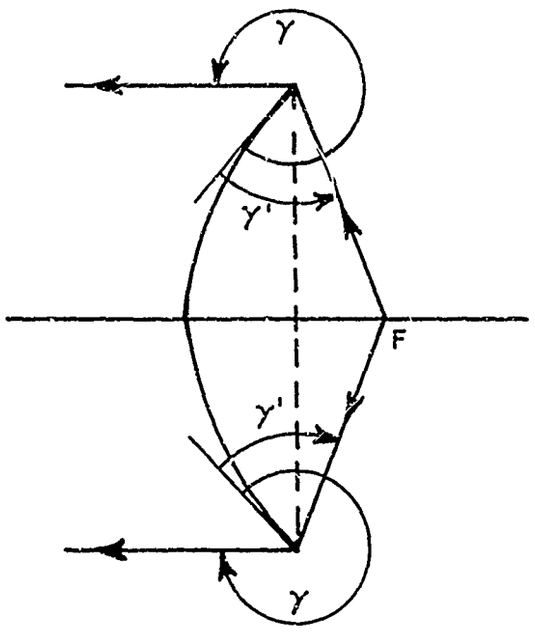

(a)
REFLECTOR ANTENNA AND RAYS FORMING
REAR AXIAL CAUSTIC

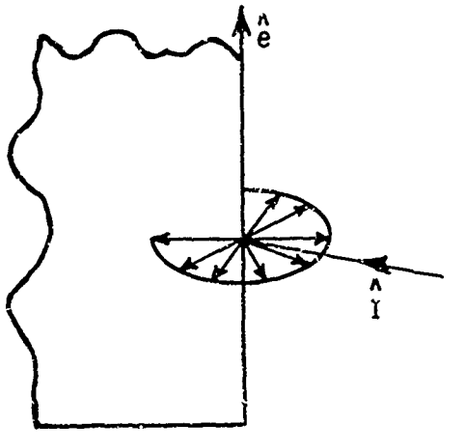

(b)
DIFFRACTION AT
HALF-PLANE

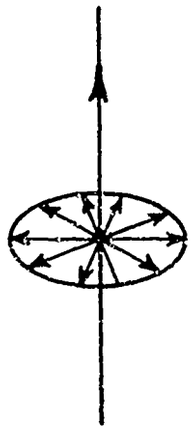

(c)
EQUIVALENT EDGE
CURRENT

Figure 8.

If the pattern of feed is relatively uniform we may functionally interpolate between E-plane and H-plane patterns. The type of interpolation used in this analysis is described below:

$$E^f(\varphi') = E_e^f(\alpha) - \left[E_e^f(\alpha) - E_h^f(\alpha)\right]\cos^2\varphi' \quad (49)$$

which can be written as

$$E^f(\varphi') = T - \delta\cos 2\varphi' \quad , \quad (50)$$

where

$$T = \frac{E_e^f + E_h^f}{2} \quad , \quad (51)$$

$$\delta = \frac{E_e^f - E_h^f}{2} \quad (52)$$

Eqs. (44), (46) and (50) now yield

$$\bar{E}^e = -\frac{a}{\sqrt{\lambda}}\frac{e}{R}^{-j(kR - \frac{\pi}{4})} D_s \int_0^{2\pi} (T-\delta\cos 2\varphi')e^{jka\sin\theta\cos(\varphi-\varphi')}\cos\varphi' \, (\hat{R}\times\hat{R}\times\hat{\varphi}')\,d\varphi' \quad , \quad (53)$$

and similarly, Eqs. (45), (47) and (50) yield

$$\bar{E}^m = -\frac{a}{\sqrt{\lambda}}\frac{e}{R}^{-j(kR - \frac{\pi}{4})} D_h \int_0^{2\pi} (T-\delta\cos 2\varphi')e^{jka\sin\theta\cos(\varphi-\varphi')}\sin\varphi' \, (\hat{R}\times\hat{\varphi}')\,d\varphi' \quad , \quad (54)$$

where $D_s = D_s(\gamma,\gamma')$ and $D_h = D_h(\gamma,\gamma')$ as mentioned earlier.

The vector products appearing in the integrals are different for the two principal planes and therefore, the evaluation of the integrals is carried out for the E- and H-planes separately.

a) E-plane Analysis

In the E-plane $\left(\varphi = \frac{\pi}{2}\right)$ the vector product appearing in the integral of Eq. (53) can be expressed in the form

$$\hat{R}\times\hat{R}\times\hat{\varphi}' = \hat{x}\sin\hat{\varphi}' - \hat{\theta}\cos\theta\cos\varphi' \quad (55)$$

Employing this relationship in Eq. (53) it is found upon evaluating the integral that the x-component vanishes and the $\hat{\theta}$- component, denoted by $F^e(\theta)$, is

$$(56) \qquad F^e(\theta) = \pi \cos\theta \left[\left(T - \frac{\delta}{2}\right) J_0(\chi) + (T-\delta)\, J_2(\chi) - \frac{\delta}{2} J_4(\chi) \right]$$

where

$$\chi = ka \sin\theta \quad ,$$

$J_m(\chi)$ is the m^{th} order Bessel function with argument χ.

Eq. (53) can now be written as

$$(57) \qquad \bar{E}^e = \hat{\theta} \frac{a\pi}{\sqrt{\lambda}} D_s \cos\theta \frac{e^{-jkR}}{R} \left[\left(T - \frac{\delta}{2}\right) J_0(\chi) + (T-\delta)\, J_2(\chi) - \frac{\delta}{2} J_4(\chi) \right] e^{j\frac{\pi}{4}}$$

Returning to Eq. (54), for the E-plane the vector product inside the integral can be expressed in the form

$$(58) \qquad \hat{R} \times \hat{\varphi}' = - \hat{x} \cos\theta \cos\varphi' - \hat{\theta} \sin\varphi' \quad .$$

Again the $\hat{x}$-component vanishes on evaluating the integral leaving only the $\hat{\theta}$-component which is given as

$$(59) \qquad F^m(\theta) = - \pi \left[\left(T + \frac{\delta}{2}\right) J_0(\chi) - (T+\delta)\, J_2(\chi) + \frac{\delta}{2} J_4(\chi) \right] \quad .$$

Thus Eq. (54) reduces to

$$(60) \qquad \bar{E}^m = - \hat{\theta} \frac{\pi a}{\sqrt{\lambda}} D_h \frac{e^{-j\left(kR - \frac{\pi}{4}\right)}}{R} \left[\left(T + \frac{\delta}{2}\right) J_0(\chi) - (T+\delta)\, J_2(\chi) + \frac{\delta}{2} J_4(\chi) \right] .$$

Employing Eqs. (57) and (60) in Eq. (48),

$$(61) \qquad \bar{E} = - \hat{\theta} \frac{\pi a}{\sqrt{\lambda}} \frac{e^{-j\left(kR - \frac{\pi}{4}\right)}}{R} \left[A_1 J_0(\chi) + A_2 J_2(\chi) + A_3 J_4(\chi) \right] \quad ,$$

where

$$(62a) \qquad A_1 = T(D_h - D_s \cos\theta) + \frac{\delta}{2} (D_h + D_s \cos\theta) \quad ,$$

$$(62b) \qquad A_2 = -T(D_h + D_s \cos\theta) - \delta\, (D_h - D_s \cos\theta) \quad ,$$

$$(62c) \qquad A_3 = \frac{\delta}{2} (D_h + D_s \cos\theta) \quad .$$

b) H-plane Analysis

In the H-plane $\phi = 0, \pi$ and the vector product

$$\hat{R} \times \hat{R} \times \hat{\phi}' = -\hat{y} \cos\phi' + \hat{\theta} \sin\phi' \cos\theta, \tag{63}$$

and

$$\hat{R} \times \hat{\phi}' = -\hat{y} \cos\theta \sin\phi' - \hat{\theta} \cos\phi'. \tag{64}$$

Substituting Eq. (63) in Eq. (53) and evaluating the integral, the contribution from the θ-component vanishes leaving

$$\overline{E}^e = \hat{y} \frac{\pi a}{\sqrt{\lambda}} D_s \frac{e^{-j(kR - \frac{\pi}{4})}}{R} \left[(T - \tfrac{\delta}{2}) J_o(\chi) - (T-\delta) J_2(\chi) - \tfrac{\delta}{2} J_4(\chi)\right] . \tag{65}$$

Next evaluating the integral in Eq. (54) after substituting Eq. (64) in the equation, we obtain the y-component as

$$\overline{E}^m = -\hat{y} \frac{\pi a}{\sqrt{\lambda}} D_h \cos\theta \frac{e^{-j(kR - \frac{\pi}{4})}}{R} \left[(T + \tfrac{\delta}{2}) J_o(\chi) + (T+\delta) J_2(\chi) + \tfrac{\delta}{2} J_4(\chi)\right] . \tag{66}$$

The total field is obtained as earlier by superposing $\overline{E}^e$ and $\overline{E}^m$ obtained above. Thus

$$\overline{E} = \hat{y} \frac{\pi a}{\sqrt{\lambda}} \frac{e^{-j(kR - \frac{\pi}{4})}}{R} \left[B_1 J_o(\chi) + B_2 J_2(\chi) + B_3 J_4(\chi)\right] , \tag{67}$$

where

$$B_1 = T(D_s - D_h \cos\theta) - \frac{\delta}{2} (D_s + D_h \cos\theta), \tag{68a}$$

$$B_2 = -T(D_s + D_h \cos\theta) + \delta(D_s - D_h \cos\theta), \tag{68b}$$

$$B_3 = \frac{\delta}{2} (D_s + D_h \cos\theta). \tag{68c}$$

The rear axis is common to both the E- and H-planes and therefore, we expect both these planes to give identical results corresponding to this direction. This has been found to be so, with the rear axial field given by

$$\overline{E}(\pi) = \hat{y} \frac{\pi a}{\sqrt{\lambda}} \left[(T - \tfrac{\delta}{2}) D_s + (T + \tfrac{\delta}{2}) D_h \right] \frac{e^{-j(kR - \frac{\pi}{4})}}{R} \tag{69}$$

III. MAIN LOBE AND ADJACENT SIDE LOBES

In this chapter a description of the aperture-field method and its application to compute the fields in the forward axial region are given. The aperture blockage caused by the feed structure and its effect on the radiation pattern are also discussed.

A. Methods of Calculation

The forward axis of a reflector of revolution with axial illumination is a caustic of the diffracted rays; moreover in the case of a parabolic antenna one also has a congruence of the ordinary reflected rays. Consequently, geometrical optics and the geometrical theory of diffraction fail at and near the forward axial direction, and as in the case of the rear axial caustic, we calculate the field in the neighborhood of forward aspect from an integral representation.

One may calculate the field of the reflector antenna in the forward axial region either from the current induced on the surface of the reflector (current-distribution method) or from equivalent sources in the aperture of the reflector (aperture-field method). In the current-distribution method the electric current flowing on the surface of the reflector is approximated by the geometrical optics current

$$\bar{J}_s(\bar{R}') = 2\,\hat{n} \times \bar{H}^f(\bar{R}') \tag{70}$$

where here $\bar{R}'$ is the position vector of a point on the surface of the reflector, $\hat{n}$ is a unit normal to the surface at $\bar{R}'$ and $\bar{H}^f(\bar{R}')$ is the magnetic field of the feed at $\bar{R}'$. The calculation of the far field of the reflector from $\bar{J}_s$ is not easy. In the case of the parabolic reflector, a simple approach is to be found in the aperture-field method described in this chapter. In the aperture-field method geometrical optics is used to determine the aperture field in terms of the field of the feed, taking into account the reflection which occurs at the surface of the reflector.

Both of these approaches have been discussed and compared by Silver, see Chapters 5 and 12 in [5]. The current-distribution method is clearly the more accurate method; however, as the diameter of the aperture in terms of a wavelength increases, the pattern calculated from the current-distribution method approaches the pattern calculated from the aperture-field method. This approach is particularly rapid in the forward axial region, and as a result the aperture-field method can be used to calculate the pattern of most aperture sizes of practical interest in the forward axial region. This conclusion is also supported by the work of Tartakovskii[7] who shows patterns calculated by the two methods; in the forward axial region they are seen to agree well. However, in the case of very deep reflectors with $f/D <$ about .25 it may be necessary to use the current-distribution method.

B. The Aperture-Field Distribution

As mentioned earlier, the forward axial fields are computed here for the case of a parabolic reflector only; however the method can be applied to reflectors of other shapes also. Figure 9 shows the configuration of the ray system employed to determine the aperture field. Consider a tube of rays emanating from the feed F located at the focal point of the reflector; this tube of rays is reflected from the surface at QQ' and appears at PP' in the aperture. The intensity of this tube of rays at PP' is obtained from the principle of power conservation in a tube of rays. Let the intensity of the reflected field at PP' be $|E^a|$. The intensity of the incident field at the surface of the reflector is $|E^f(R')|$. Therefore, according to the principle of power concentration in a tube of rays

$$|E^f(R')|^2 \, R' \, d\psi \, \rho' \, d\phi' \, d\rho' = |E^a|^2 \, d\rho' \, \rho' \, d\phi'; \tag{71}$$

which reduces to

$$|E^a| = |E^f(R')| \sqrt{R' \frac{d\psi}{d\rho}} \, . \tag{72}$$

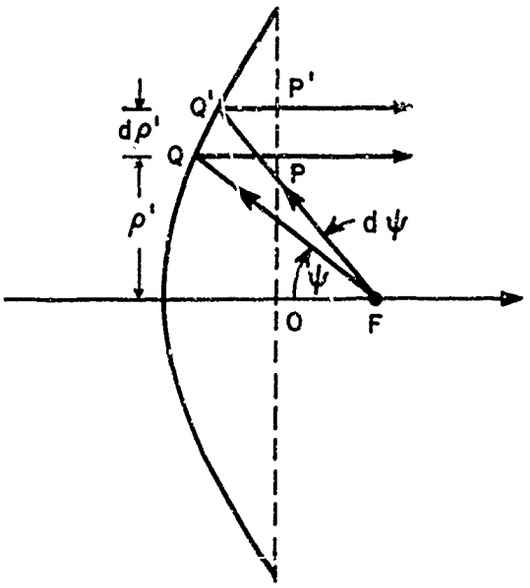

Fig. 9 - Rays used to calculate the aperture field distribution.

For the paraboloid of revolution with focal distance f

$$\psi = \tan^{-1} \frac{\rho'}{f - \frac{\rho'^2}{4f}} \quad , \tag{73}$$

which yields

$$\frac{d\psi}{d\rho'} = \frac{1}{f + \frac{\rho'^2}{4f}} = \frac{1}{R'} \tag{74}$$

so that employing Eqs. (6), (9), (72) and (74)

$$|E^a| = \frac{A\, f(\psi,\varphi')}{R'} \quad . \tag{75}$$

Finally adding polarization and phase information

$$\overline{E}^a(\rho',\varphi') = \hat{y}\, A\, h(\rho',\varphi') \frac{e^{-jkR_o}}{R'} \quad , \tag{76}$$

where

$$-h(\rho',\varphi') = f(\psi,\varphi') = g(\theta_f,\varphi_f) \quad ,$$

R_o is the distance from the focus to the edge of the reflector.

The normalizing constant A is chosen so that the amplitude of the electric field in the center of the aperture is unity. Since $h_{(o)} = 1$, A = f the focal distance, and

$$\overline{E}^a(\rho',\varphi') = \hat{y}\, f\, h(\rho',\varphi') \frac{e^{-jkR_o}}{R'} \tag{77}$$

Even though it has been assumed that the feed radiation is linearly polarized in the y direction, the aperture field is in general not linearly polarized due to the curvature of reflecting surface. The aperture field has a cross polarized component in the x direction which vanishes in the two principal planes leaving only the y component. It is also seen that the direction of the x component reverses as one moves from one quadrant to the adjacent one; see Fig. 12.2 in [5]. Furthermore, the magnitude of this component is small compared to the y component. Therefore, these cross polarized fields do not really contribute to the far zone field in the two principal planes; however they give rise to small cross-polarized lobes in the axial planes at 45° to the principal planes.[21]

As mentioned earlier $h(\rho'\varphi')$ may be determined from calculation or a series of pattern measurements; however in many cases it suffices to measure the field of the feed in its E- and H-planes and to determine the field of the feed elsewhere by the functional interpolation scheme described on page 21.

Thus the aperture electric field is given by

$$\bar{E}^a(\rho',\varphi') = \hat{y}\left[\bar{E}^a_e(\rho') - [\bar{E}^a_e\,\rho') - \bar{E}^a_h(\rho')]\cos^2\varphi'\right] \tag{78}$$

This can be written in terms of T and δ [Eqs. (51) and (52)], both of which are functions of ρ'. Consequently,

$$\bar{E}^a(\rho',\varphi') = \hat{y}\,[T(\rho') - \delta(\rho')\cos 2\varphi'] \tag{79}$$

C. Integral Representation of the Field

The integral representation of the far zone of a radiating system is described in App. III. If we completely enclose the reflector by the dotted surface S as shown in Fig. 10, and if the exact values of the equivalent currents $\bar{J}_S = \hat{n} \times \bar{H}$ and $\bar{K}_S = \bar{E} \times \hat{n}$ are known everywhere on S, then the radiation from the reflector can be found exactly. However, in the present case the reflector diameter is taken to be large in terms of a wavelength; consequently. we may employ the following approximations in calculating the reflector far zone field in the forward axial region.

1) $\bar{J}_S = o$ on the back side of the reflector,

2) $\bar{K}_S = \bar{E}^a \times \hat{z}$, where $\bar{E}^a$ is given by Eq. (79),

3) $\bar{J}_S = \hat{z} \times \bar{H}^a$, where $\bar{H}^a = \dfrac{\hat{z} \times \bar{E}^a}{Z_o}$.

In addition, the approximations $\hat{R} \cdot \hat{z} = \cos\theta \approx 1$ and $\sin\theta \approx 0$ may be used in the amplitude of the integrand of the radiation integral, with the result that the far zone electric field of the reflector in the forward axial region is given to a good approximation by

$$\bar{E}(\bar{R}) \approx \hat{y}\,\frac{j}{\lambda}\,\frac{e^{-jkR}}{R}\int_A e^{jk\bar{\rho}\,\cdot\,\hat{R}}\,E^a(\bar{\rho}')\,ds' \tag{80}$$

Employing Eq. (79) this yields

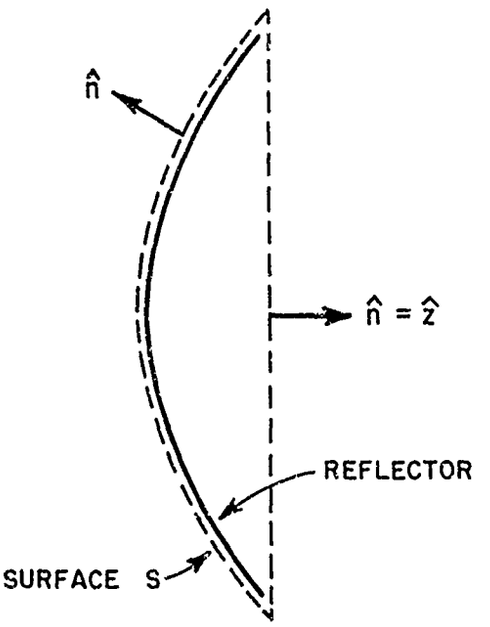

Fig. 10 - Surface of integration for the aperture-field method.

$$\bar{E}(\bar{R}) = \hat{y}\,\frac{j}{\lambda}\,\frac{e^{-jkR}}{R}\int_0^{2\pi}\int_0^{a}\left[T(\rho') - \delta(\rho')\cos 2\varphi'\right] e^{jk\rho' \sin\theta \cos(\varphi-\varphi')}\,\rho'\,d\rho'\,d\varphi' \tag{81}$$

Carrying out the integration with respect to φ',

$$\bar{E}(\bar{R}) = \hat{y}\,\frac{j}{\lambda}\,\frac{e^{-jkR}}{R}\,2\pi\int_0^{a}\left[T(\rho')\,J_0(k\rho' \sin\theta) + \delta(\rho')\cos 2\varphi\,J_2(k\rho' \sin\theta)\right]\rho'\,d\rho' \tag{82}$$

in which J_0 and J_2 are Bessel functions of order 0 to 2 respectively. If one considers the two principal planes only, the cos 2φ term inside the integral takes the value -1 for the E-plane and +1 for the H-plane. T and δ can be expressed in terms of the known functions $f_e(\psi) = h_e(\rho')$ and $f_h(\psi) = h_h(\rho')$ using Eqs. (51), (52) and (77), as

(83) $$T(\rho') = \frac{f}{2R'} e^{-jkR_o} [h_e(\rho') + h_h(\rho')]$$

(84) $$\delta(\rho') = \frac{f}{2R'} e^{-jkR_o} [h_e(\rho') - h_h(\rho')] \quad .$$

The expressions for h_e and h_h may be found from the measured feed patterns and the integration in Eq. (82) can then be evaluated numerically by the Simpson's method. To avoid cumulative errors forty points per wavelength are taken in the integration, which is repeated at half degree intervals. The far zone pattern is normalized to the main beam maximum value, which is taken to be 0 dB.

D. The Aperture Blockage

The presence of the feed and its support in the path of the reflected rays has not been taken into account in the preceding analysis. One can expect that this will give rise to wide angle scattering and therefor increase the side lobe levels while reducing the gain slightly. Because of the complicated nature of the feed structure, which includes the actual radiator and its supporting structure, an exact analysis of the contribution made by the aperture blockage is a difficult task. However, an approximate assessment of the increase in side lobe levels in the forward region can be made if one assumes that the feed blocks out a portion of the aperture radiation equal to its physical cross section, as viewed from the forward axial direction. In other words, one assumes that the feed gives rise to a shadow in the aperture field in the geometrical optics sense. This is the customary method of approximating the effect of aperture blockage. In the second example treated here, there is a significant aperture blockage; in this case the shadow area can be approximated by a circle of radius c. Since the shadow area is located at the center of the reflector aperture and is relatively small, the aperture field here is approximately equal to unity. The far field set-up by this "shadow" aperture can be written as

(85) $$\bar{E}_s = - \hat{y} \frac{j}{\lambda} \frac{e^{-jkR}}{R} 2\pi c^2 \frac{J_1(kc \sin\theta)}{kc \sin\theta} e^{-jkR_o}$$

where J_1 is the Bessel function of order 1. The resultant field in the forward axial region can then be obtained by the super-position of Eqs. (82) and (85).

Since the hypothetical shadow aperture is small compared with the reflector aperture, its pattern given by Eq. (85) will be very broad describing a background radiation in the forward axial region which is roughly constant and opposite in phase to the reflector pattern on axis.

IV. MEASUREMENTS

In order to check the theoretical analysis given in the previous chapter measurements were taken on a parabolic reflector antenna operating in the X-band range of frequencies. A description of the antenna, the antenna range and the E- and H-plane patterns obtained for the primary field of the feed are presented in this chapter.

A. Description of the Antenna

The antenna used to obtain the far field power patterns (Figs. 15 and 16) is shown in Fig. 11. The diameter of the aperture of the parabolic reflector is 24.0 inches and its focal length is 8.0 inches. The edge of the surface has a thickness of 0.057 inch which can be considered small compared with the measurement wavelength. The feed is an open-ended flanged rectangular waveguide. The feed support consists of a tripod which is fabricated of polystyrene. The cylindrical legs of this tripod are 0.37 inch in diameter and are mounted well away from the edge of the reflector to minimize interference with the edge diffraction. A simple tuner in the form of a waveguide plunger is employed to match the feed to a crystal mixer. The i-f output of the mixer is fed to a coaxial transmission line, which is attached to one of the legs of the tripod.

The position of the feed was carefully checked to ensure that its effective phase center was at the focal point of the reflector. It was first positioned mechanically, then finally adjusted to obtain: 1) a maximum radiated signal in the forward axial direction, 2) a pattern symmetrical about the reflector axis. It was found that the focus of the reflector is about 0.1 inch behind the aperture of the feed.

B. The Antenna Range

An outdoor antenna range was employed. The patterns of the reflector antenna were measured at a range of 45 feet, which corresponds to $R = D^2/\lambda$, here D is the aperture diameter. A block diagram of the antenna measuring system is shown in Fig. 12.

The transmitter consists of a frequency stabilized X-13 klystron. The transmitted power is approximately 150 milliwatts, and the measurement frequency is 11 Ghz. The transmitter feeds a horn which has corrugated inner walls to minimize its side lobe level. The horn has a gain of about 20 db, and its half power beam widths are approximately 15 degrees in the E- and H-planes. The horn is mounted about 13 feet above the ground. The parabolic antenna is mounted at the top of a metal mast 6 feet long and 1.75 inches in diameter. The mast in turn is mounted on a pedestal whose height and axis rotation are adjustable. The rotation of the pedestal is controlled from a panel by a selsyn system; a second selsyn system controls the rotation of the recorder

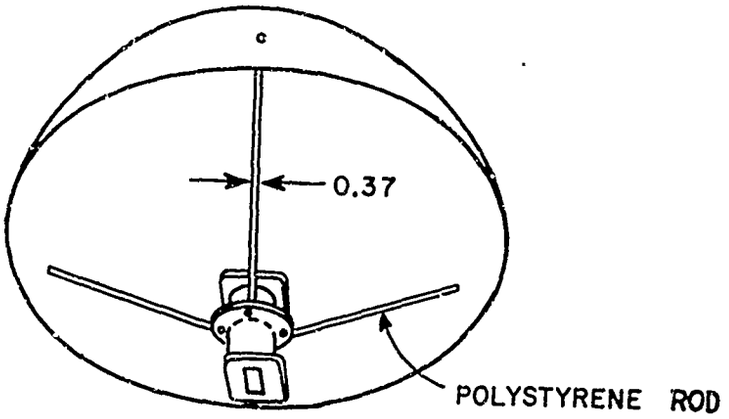

(a)

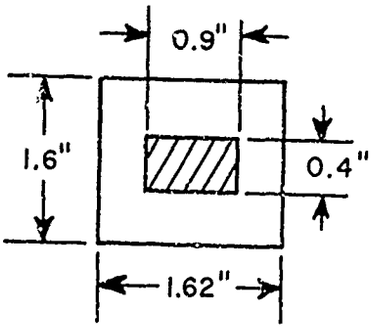

(b)

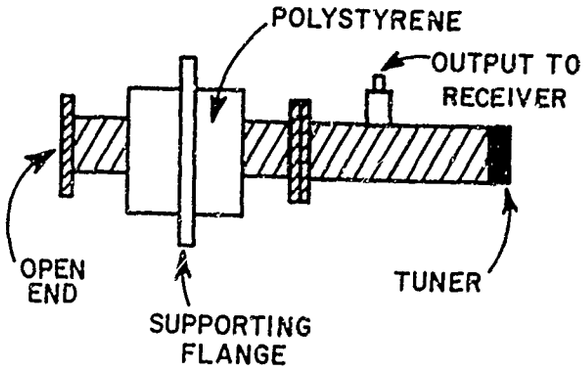

(c)

Fig. 11. Description of the parabolic reflector antenna used in the measurements.

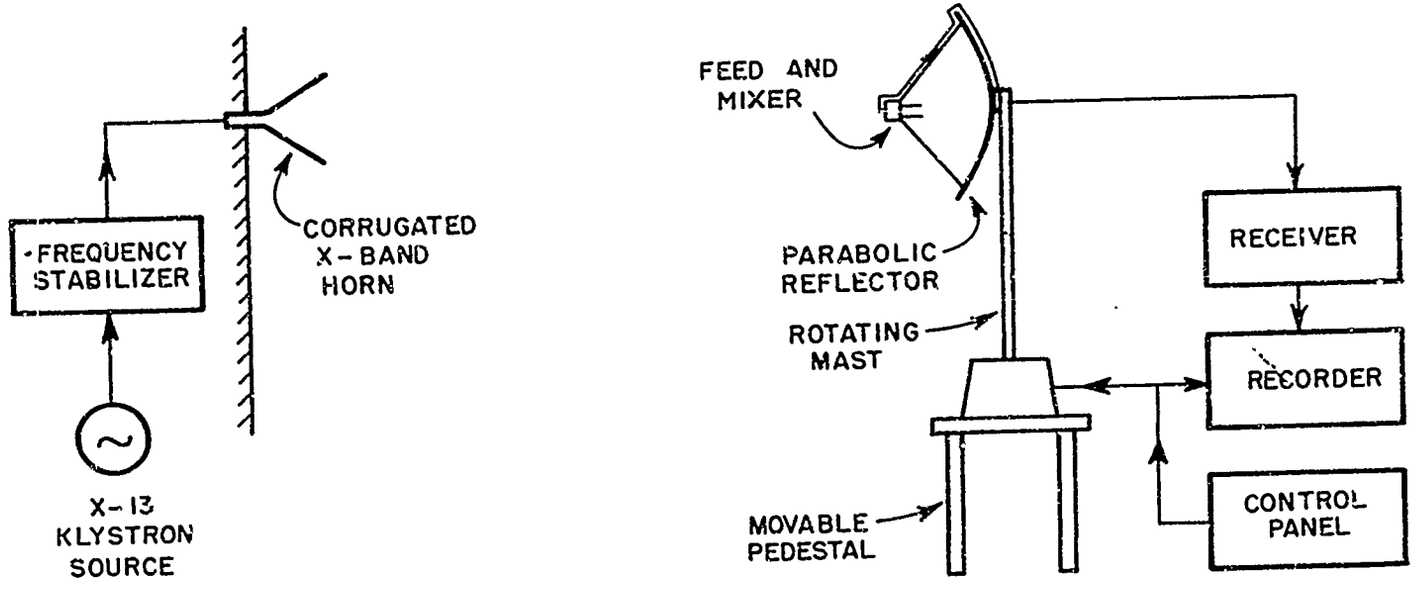

Fig. 12 - Diagram of the antenna measuring system.

drum from the panel. In recording the patterns, two degrees of antenna rotation correspond to one inch of recorded pattern. Before a pattern measurement, both the height of the antenna and the orientation of the axis of rotation of the mast were carefully checked to make certain the range was aligned.

The i-f output of the parabolic antenna is fed to a Scientific-Atlanta series 1600 receiver, which in turn is connected to a Scientific-Atlanta series 1520 recorder. The receiving system, including the crystal mixer at the antenna feed, has a sensitivity of about -96 dbw at 11 Ghz. In principle, the antenna measuring system is sensitive enough to record the complete E- and H-plane patterns of the parabolic antenna at a 45 feet range. In other words, the transmitter power level and receiver noise level are not a limitation to pattern measurement. Satisfactory E-plane patterns were recorded. Also satisfactory H-plane patterns were recorded, except for the deep shadow region behind the reflector; there only the primary lobe of the rear axial caustic was strong enough to be measured without interference from a background signal. These measured E- and H-plane patterns are compared with calculated patterns in the next chapter.

During the measurement of the pattern behind the reflector, the main beam illuminates a field of closely mowed grass. Rough calculations show that the terrain backscatter from this field of grass is about the same order of magnitude as the H-plane signal received behind the reflector. It is believed that this terrain scatter is the spurious background signal mentioned in the preceding paragraph.

C. The Primary Feed Patterns

The patterns of the primary feed also were measured at a range of 45 feet. The flanged waveguide feed supports only dominant TE_{01} mode, so that it produces a linearly polarized field. The measured patterns in both E- and H-planes are shown in Fig. 13. It is seen that the E-plane pattern has a taper of about 13 db, and the H-plane pattern a taper of about 16 db at angular distances corresponding to the reflector edge. The beam widths at the 3 db level are 66° and 56° in the E- and H-planes, respectively. The patterns are roughly similar to those calculated from theoretical formulas for the unflanged open-end rectangular waveguide, assuming that no reflected waves exist at the guide termination.[22] However, these formulas were not used in the analysis as the representation of the primary feed pattern; it was found to be rather critical in determining the secondary pattern. Therefore, the measured primary patterns in both E- and H-planes were represented closely by empirical formulas, so that they could be employed to interpolate the values at each of the points used in the integration of Eq. (82). For the E-plane a good empirical expression is given by

$$f_e(\psi) = e^{-3.5 \times 10^{-4} \psi^2 + 1.3 \times 10^{-8} \psi^4} \tag{86}$$

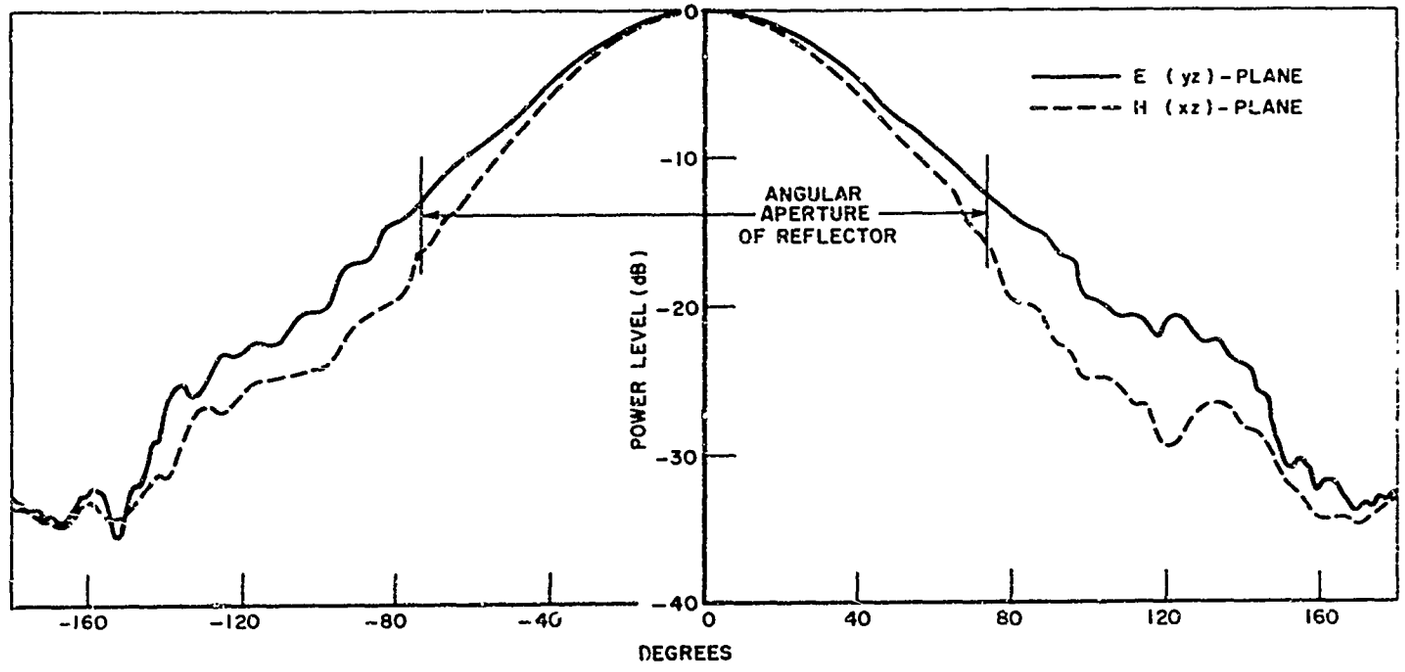

Fig. 13 - Measured primary field patterns of a flanged waveguide feed.

and the the H-plane

$$f_h(\psi) = e^{-4.4 \times 10^{-4} \psi^2 + 2.0 \times 10^{-8} \psi^4} \tag{87}$$

where ψ is measured in degrees. These formulas are valid only in the forward region of the feed where the patterns have a monotonic behavior.

V. RESULTS AND DISCUSSION

The methods developed earlier are applied to calculate the patterns of two parabolic reflector antennas. One of them is the same antenna described in the last chapter, the other is a parabolic reflector with a dipole feed. A comparsion of the calculated patterns is presented in this chapter, and some conclusions are reached concerning the utility of the geometrical theory of diffraction in this type of problem.

The scattering from the feed and its support are only approximated crudely, see section 3.4; therefore it is desirable in evaluating the present method of analysis to begin with a case where the scattering from the feed and its support is minimal. In such a case we can see how well this method predicts the wide angle radiation from the reflector.

A. Parabolic Reflector with Dipole Feed

Afifi[10] has measured the H-plane pattern of a parabolic antenna mounted on a ground plane. The feed consists of a dipole positioned at the focus, which lies in the aperture of the reflector In this configuration there is no scattering from the feed suppor and the scattering from the feed itself is relatively small compared with the edge diffraction and direct feed radiation.

The aperture diameter is 10.65λ and f/D ratio is 0.25. Afifi's measured pattern is compared with a pattern calculated from computer programs based on the two point and ring current methods; the pattern calculated by the latter method blends smoothly with that calculated by the former method at $\theta = 168^{\circ}$. The pattern in the forward axial region was not calculated as it would simply coincide with that calculated by Afifi, who used the current-distribution method. At the shadow boundary the secondary pattern is 6 dB below that of the primary pattern; this was used to relate the levels of the calculated and measured patterns shown in Fig. 14.

The agreement between calculated and measured patterns is excellent between the forward axial region and the shadow boundary of the reflector (from 10° to 90°) and also in the shadow region behind the reflector from 90° to 130°. The agreement in the deep shadow region at aspects greater than 130° is good. Based upon previous experience with pattern measurement in the deep shadow region, it is safe to attribute a good part discrepancy here to measurement error at these low signal levels, see the discussion on page 33. Thus, in general, this comparison between calculated and measured patterns is very gratifying, because it confirms the accuracy of our solution based upon the geometrical theory of diffraction.

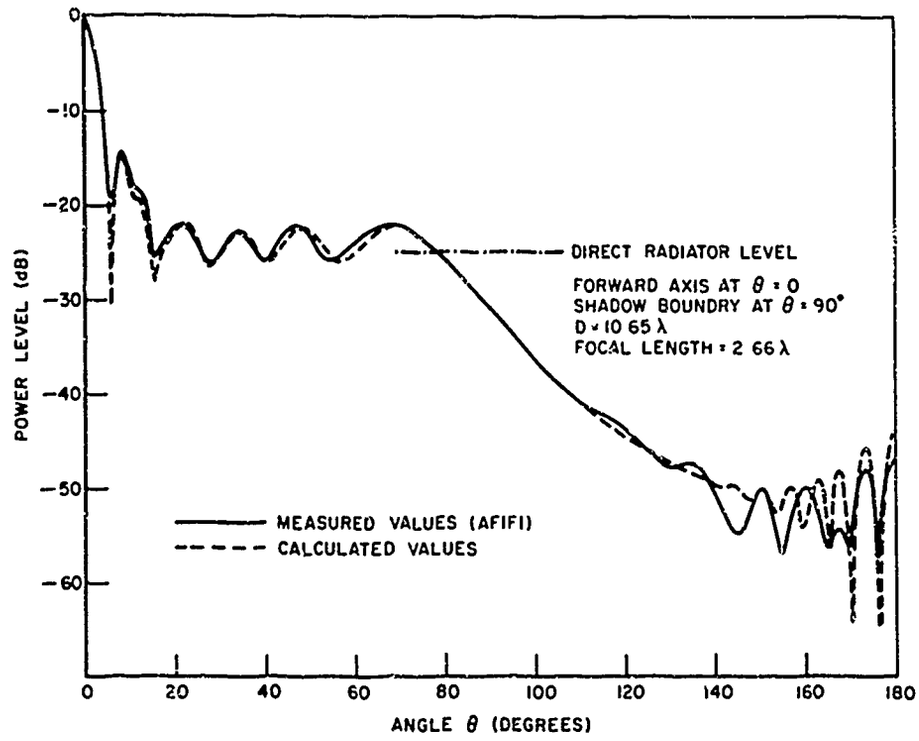

Fig. 14 - H-plane pattern of a parabolic reflector with a dipole feed.

B. Parabolic Reflector with Flanged Waveguide Feed

This antenna and the measurement of its patterns, together with the patterns of its feed, are described in Chapter IV. The patterns are calculated from computer programs which are based on all of the analytical methods described in Chapters II and III, including the aperture blockage due to the feed alone. The pattern calculations for the forward and rear axial regions are joined smoothly with those calculated by the two point method.

The calculated and measured E-plane patterns are compared in Fig. 15. The patterns were first calculated neglecting aperture blockage (solid curve), and then the effect of aperture blockage was included (dotted curve) in the region between 0 and 25 degrees. It was felt that the nature of the approximation did not justify the inclusion of aperture blockage at the larger aspect angles. In part, this belief was based on the fact that the scattering from the dielectric rods contributes perceptibly at the larger aspect angles, and this was not included in the analysis.

The power level of the main beam maxima of the three patterns is chosen to be 0 dB, and it is clear that the calculated patterns predict the shape of the main beam well, as one would expect. The calculated and measured patterns also are in very good agreement in the region behind the reflector, where aperture blockage does not affect the pattern directly. The close agreement of the lobe structure of the two patterns in this region again confirms the accuracy the analysis based on the geometrical theory of diffraction. This agreement is all the more remarkable when one notes that it occurs at pattern levels which are 40 to 50 dB down with respect to the main beam maximum.

In the illuminated region, between 30° and the shadow boundary at 107°, the calculated and measured patterns are in fairly good agreement. In the region between 5° and 30° the agreement is poor unless the effect of aperture blockage is included. The calculation without aperture blockage is of interest in the region between 5° and 30°, because it indicates the minimum achievable side lobes in the region close to the main beam, for a given aperture illumination. Any significant aperture blockage raises the level of these side lobes.

In the H-plane the aperture taper is 3 dB greater than that in the E-plane; furthermore, the orientation of the dielectric rods of the tripod with respect to the polarization of the feed is such as to result in a somewhat greater scattering from the tripod. Thus one would expect larger discrepancies between the calculated and measured patterns in this plane, and this expectation is confirmed in Fig. 16, where the overall agreement between the two patterns is only fair. Despite the absence of detailed agreement, the general behavior of the measured pattern is predicted qualitatively by the calculated pattern; this observation is particularly true when one notes that the comparison is made over a dynamic range exceeding 60 dB.

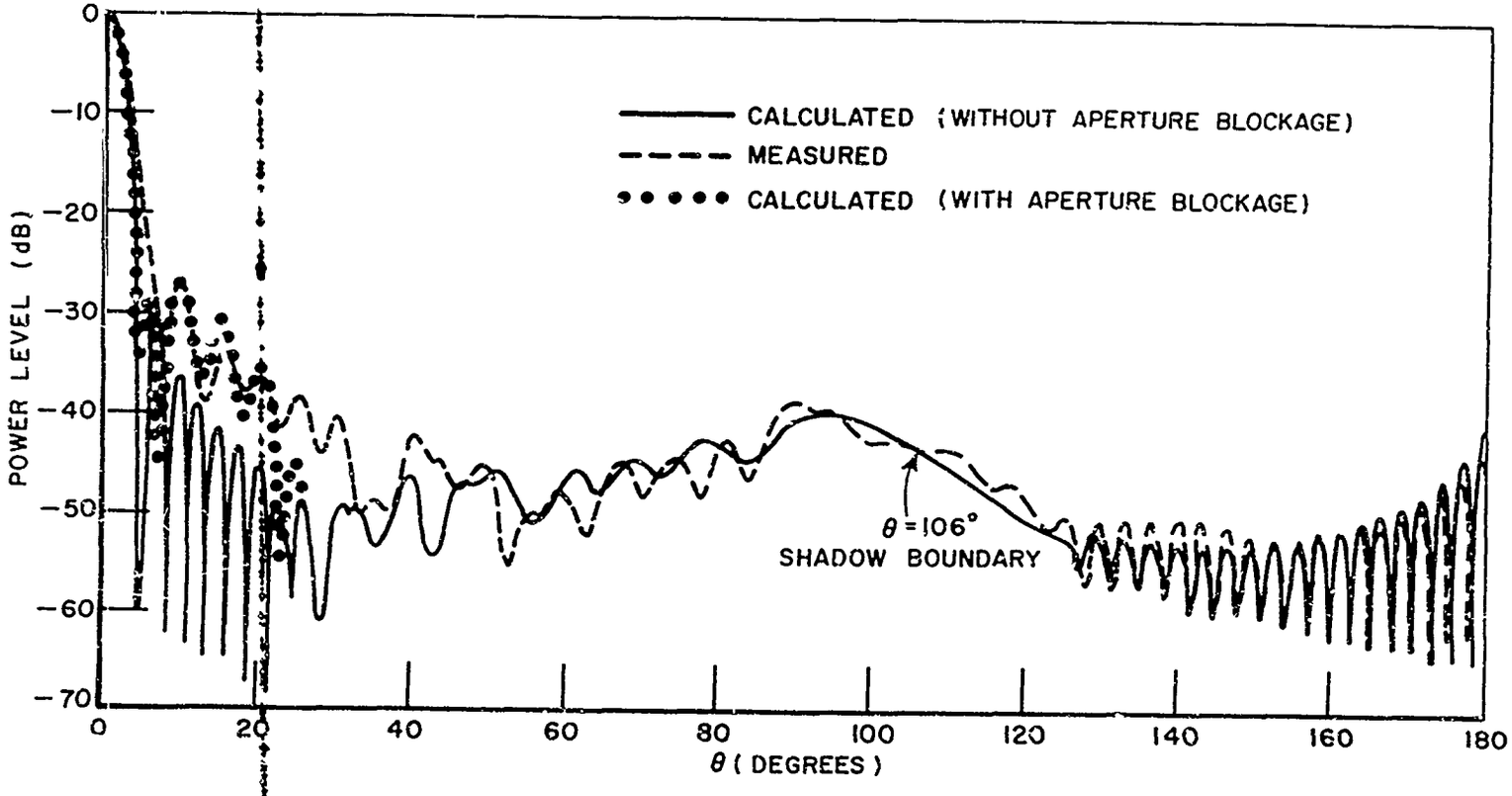

Fig. 15. E-plane pattern of a parabolic reflector with a flanged waveguide feed.

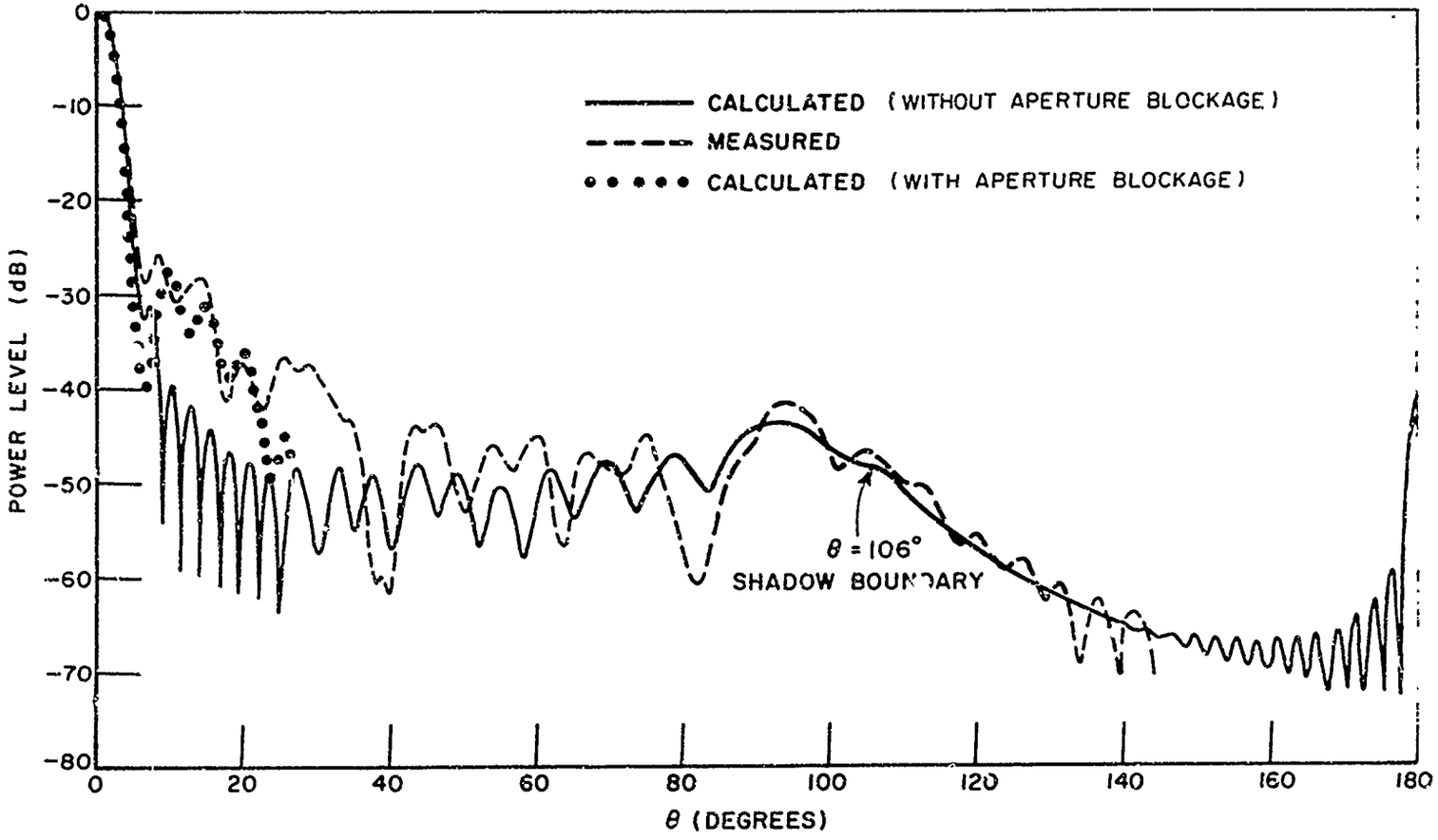

Fig. 16. H-plane pattern of a parabolic reflector with a flanged waveguide feed.

As in the case of the E-plane pattern, the shape of the main beam is predicted well from the aperture-field method. Also the shape of the main lobe of the rear axial caustic is predicted well by the theory. The minor lobe structure in the deep shadow region behind the reflector was too low to be measured accurately, and it is not included in the measured pattern.

It is evident from the above discussion that the scattering from the feed and its support can play an important part in determining the side lobes of a reflector antenna; hence it is desirable to extend the present solution to include a careful analysis of this effect.

C. Wide Angle Side Lobes

The following observations concerning the characteristics of the wide angle side lobes of a parabolic reflector antenna are based on the two examples described here. In the region between the forward axial region and the shadow boundary the wide angle side lobes depend upon the direct feed radiation, the edge diffracted radiation, and the aperture blockage if it is significant. The average level of these side lobes is closely related to the feed pattern. There is a pattern maximum near the shadow boundary which results from the in phase combination of the feed radiation and the edge diffracted radiation. The edges of both reflectors are sharp; hence the field at the shadow boundary is 6 dB below the feed field illuminating the edge.

The field drops sharply as one enters the shadow region. In the deep shadow region the many well defined lobes of the measured pattern shown in Fig. 15 confirm the radiation mechanism associated with the two edge diffracted rays. Finally, we note that there is another pattern maximum at the rear axial caustic. The fields diffracted at the edge of the reflector in the vicinity of the E-plane are primarily responsible for this relatively large pattern maximum. It can be eliminated by placing a limited amount of absorber at appropriate positions on the rim of the parabola.[14] Also, this same absorber will reduce the deep shadow pattern of Fig. 15 to roughly that of Fig. 16. This illustrates the usefulness of the geometrical theory of diffraction solution in antenna design, which stems from its direct association with the radiation mechanism.

D. Conclusions

The complete pattern of a parabolic reflector antenna can be calculated using the singly-diffracted rays of the geometrical theory of diffraction, with proper corrections for the forward and real axial directions. Excellent agreement with experimental patterns can be expected, if the aperture blockage is not significant.

The solution has the usual advantages of a solution based on the geometrical theory of diffraction, namely, it is obtained in the form of simple functions, its computation cost is low, it is directly related to the radiation mechanism of the antenna so it can be readily used in the design problem, and it can be easily extended and modified as the need arises.

APPENDIX I

HALF-PLANE DIFFRACTION COEFFICIENT

The dyadic diffraction coefficient $\overline{\overline{D}}$ for the half-plane can be expressed in terms of the two scalar diffraction coefficients D_s and D_h for the soft and hard boundary conditions, respectively. Let the total scalar field U be the sum of a geometrical optics field and a diffracted field U^d. At the surface of the half-plane U = 0 for the soft boundary condition, whereas $\partial U/\partial y = 0$ for the hard boundary condition, see Figure 17. The diffraction of a scalar plane wave field by a half-plane has been solved exactly by Sommerfeld;[23] recently Pathak and Kouyoumjian[24] have obtained an asymptotic solution for the spherical wave illumination of the wedge. This solution is particularly amenable to interpretation in terms of the geometrical theory of diffraction. In this appendix we reproduce the results of their solution only for the half-plane and for the illumination of the edge at normal incidence.

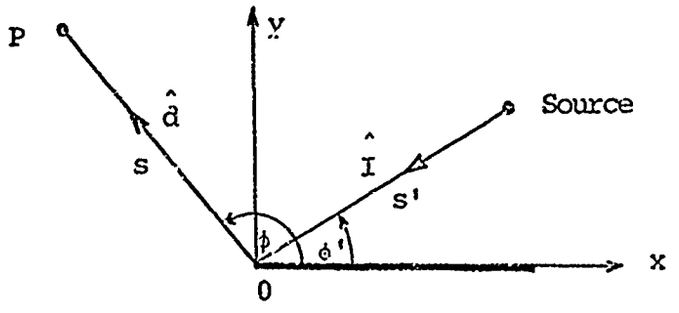

Figure 17. Half-plane diffraction in the plane which contains the source and is perpendicular to the edge.

Fig. 17 - Half-plane diffraction in the plane which contains the source and is perpendicular to the edge.

Let $U^i(s',\varphi')$ be the field of the spherical wave incident at the edge of the half-plane. The diffracted fields for the soft (s) and hard (h) boundary conditions are

$$(A1) \qquad U_{s,h}^{d}(s,\varphi) = U^i(s',\varphi')\, D_{s,h}(\varphi,\varphi') \sqrt{\frac{s'}{s(s+s')}}\, e^{-jks}$$

where the scalar diffraction coefficients are given by

$$(A2) \qquad D_{s,h}(\varphi,\varphi') = -\frac{e^{-\frac{j\pi}{4}}}{2\sqrt{2\pi k}}\left[\frac{F(kLa_-)}{\cos\frac{\varphi-\varphi'}{2}} \mp \frac{F(kLa_+)}{\cos\frac{\varphi+\varphi'}{2}}\right],$$

with

$$(A3) \qquad F(kLa_\mp) = j2\sqrt{kLa_\mp}\, e^{jkLa_\mp}\int_{\sqrt{kLa_\mp}}^{\infty} e^{-j\tau^2}\, d\tau \quad ,$$

$$(A4) \qquad a_\mp = 2\cos^2\frac{(\varphi \mp \varphi')}{2}$$

$$(A5) \qquad L = \frac{ss'}{s+s'}$$

$F(kLa_\mp)$ is a correction factor needed only in the transition regions of the reflection and shadow boundaries. Away from these boundaries, more precisely when $kLa_\mp > 10$, $F(kLa_\mp) \simeq 1$ and may be replaced by unity in Eq. (A2). It is to emphasize this behavior that we show the diffraction coefficient to be a function of φ and φ' only.

The integral appearing in this factor is related to the tabulated Fresnel integral:

$$\int_x^\infty e^{-j\tau^2}\, d\tau = \int_0^\infty e^{-j\tau^2}\, d\tau - \int_0^x e^{-j\tau^2}\, d\tau \quad ,$$

where

$$\int_0^\infty e^{-j\tau^2}\, d\tau = \sqrt{\frac{\pi}{2}}\,(0.5 - j\,0.5) \quad ,$$

and

$$\int_0^x e^{-j\tau^2}\, d\tau = \sqrt{\frac{\pi}{2}}\left[C\left(\sqrt{\frac{2}{\pi}}\,x\right) - j\,S\left(\sqrt{\frac{2}{\pi}}\,x\right)\right],$$

C and S being the tabulated Fresnel integrals of argument $\sqrt{\frac{2}{\pi}}\,x$. Thus

$$(A6) \qquad \int_x^\infty e^{-j\tau^2}\, d\tau = \sqrt{\frac{\pi}{2}}\left[\left[0.5 - C\left(\sqrt{\frac{2}{\pi}}\,x\right)\right] - j\left[0.5 - S\left(\sqrt{\frac{2}{\pi}}\,x\right)\right]\right]$$

The values of the functions C and S are obtained using the library subroutines available in the IBM 360/75 computer.

For rays normally incident on the edge of a perfectly-conducting half-plane the dyadic diffraction coefficient[18]

$$\bar{\bar{D}} = \hat{e}\,\hat{e}\,D_s + \hat{p}_d\,\hat{p}\,D_h \quad , \tag{A7}$$

where

$\hat{e}$ is the unit vector tangent to the edge,

$\hat{p} = \hat{e} \times \hat{I}$; $\hat{I}$ being the unit vector in the direction of the incident ray,

$\hat{p}_d = \hat{e} \times \hat{d}$; $\hat{d}$ being the unit vector in the direction of the diffracted ray.

Thus the diffracted electromagnetic field

$$\bar{E}^d(s,\varphi) = \bar{\bar{D}}(\phi,\phi') \cdot \bar{E}^i(s',\phi') \sqrt{\frac{s'}{s(s+s')}}\, e^{-jks} \tag{A8}$$

In the case of high frequency diffraction, it is interesting to note how intimately scalar diffraction is related to vector (electromagnetic) diffraction, as evidenced by the form of the dyadic diffraction coefficient.

APPENDIX II

CAUSTIC DISTANCES

Employing differential geometry a new formula has been derived[18] for the distance ρ of a caustic from the point of diffraction Q on a curved edge.

Let

ℓ be the distance from the phase center of the source to Q,

ρ_e be the radius of curvature of the edge,

$\hat{e},\hat{n}$ be the unit vectors tangent and normal to the edge directed outward from the center of curvature, respectively,

$\hat{I},\hat{d}$ be the unit vectors in the direction of the incident and diffracted rays at Q,

β be the angle between I and e.

Then

$$\frac{1}{\rho} = \frac{1}{\ell} - \frac{\hat{n} \cdot (\hat{I} - \hat{d})}{\rho_e \sin^2\beta} \tag{A9}$$

Substituting a for ρ_e, $\frac{\pi}{2}$ for β, R_o for ℓ, we get

$$\frac{1}{\rho_i} = \frac{1}{R_o} - \frac{\hat{n}_i \cdot (\hat{I}_i - \hat{d}_i)}{a} \tag{A10}$$

with i = 1, 2 corresponding to Q_1 and Q_2, respectively.

a) Diffraction at Q_1 (see Fig. 6)

$$\hat{n}_1 = y$$

$$\hat{I}_1 = \frac{\hat{y}a - \hat{z}(r-h)}{R_o}$$

$$\hat{d}_1 = \frac{\hat{z}\, R \cos\theta + \hat{y}(R \sin\theta - a)}{r_1}$$

Thus

$$\hat{n}_1 \cdot \hat{I}_1 = \frac{a}{R_o} \text{ and } \hat{n}_1 \cdot \hat{d}_1 = \frac{R \sin \theta - a}{r_1}$$

which yield

(A11) $$\rho = \frac{a\, r_1}{R \sin \theta - a}$$

b) Diffraction at Q_2

$$\hat{n}_2 = - \hat{y}$$

$$\hat{I}_2 = \frac{- \hat{y} a - \hat{z}(f-h)}{R_o}$$

$$\hat{d}_2 = \frac{\hat{z}\, R \cos \theta + \hat{y}(R \sin \theta + a)}{r_2}$$

Thus

$$\hat{n}_2 \cdot \hat{I}_2 = \frac{a}{R_o} \text{ and } \hat{n}_2 \cdot \hat{d}_2 = - \frac{(R \sin \theta + a)}{r_2}$$

which yield

(A12) $$\rho_2 = - \frac{a\, r_2}{R \sin \theta + a} \quad .$$

APPENDIX III

FAR ZONE INTEGRAL REPRESENTATION OF THE FIELD

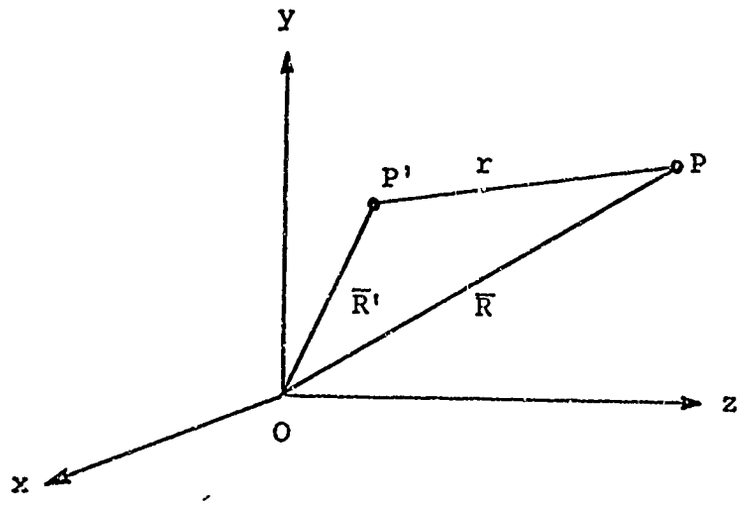

Fig. 18 - Geometry of the Source Point P' and the Field Point P.

The far zone criteria for the radiation field are given by

a) $kr \gg 1$,

b) $R \gg D'$ with $R' \leq D'$,

where

r is the distance between the source point P' and the field point P,

R' is the distance between P' and O, and

D' is the maximum distance of the source distribution from O.

These conditions lead to the following approximations in the radiation integral:

a) $r \simeq R - \bar{R}' \cdot \hat{R}$ in the calculation of phase,

b) $r \simeq R$ in the amplitude term,

c) terms of order $\frac{1}{r^2}$ and $\frac{1}{r^3}$ are neglected.

The electric field $\bar{E}$ and the magnetic field $\bar{H}$ will each be transverse to the direction of propagation $\bar{R}$ and are related by the characteristic impedance of the medium Z_o, so that

$$\bar{E} = Z_o \, \bar{H} \times \hat{R} \quad . \tag{A13}$$

The electric field due to an electric current moment $d\bar{p}_e$ is given by

$$\bar{E}^e(\bar{R}) = \frac{jkZ_o}{4\pi} \frac{e^{-jkR}}{R} \int_{\text{sources}} e^{jk\bar{R}'} \cdot \hat{R} \; \hat{R} \times [\hat{R} \times d\bar{p}_e(\bar{R}')] \quad , \tag{A14}$$

and the corresponding magnetic field follows from Eq. (A13) as

$$\bar{H}^e(\bar{R}) = - \frac{jk}{4\pi} \frac{e^{-jkR}}{R} \int_{\text{sources}} e^{jk\bar{R}'} \cdot \hat{R} \; \hat{R} \times d\bar{p}_e(\bar{R}') \tag{A15}$$

The electric field due to a magnetic current moment $d\bar{p}_m$ is obtained from the above equation by duality and is

$$\bar{E}^m(\bar{R}) = \frac{jkZ_o}{4\pi} \frac{e^{-jkR}}{R} \int_{\text{source}} e^{jk\bar{R}'} \cdot \hat{R} \; Y_o \hat{R} \times d\bar{p}_m(\bar{R}') \quad . \tag{A16}$$

The current moments for surface and line distributions of current are given by

$$d\bar{p}_e(\bar{R}') = \begin{cases} \bar{J}_s(\bar{R}') \, ds' \\ I(\ell') \, \hat{\ell}' \, d\ell' \end{cases} \quad , \tag{A17}$$

$$d\bar{p}_m(\bar{R}') = \begin{cases} \bar{K}_s(\bar{R}') \, ds' \\ M(\ell') \, \hat{\ell}' \, d\ell' \end{cases} \quad . \tag{A18}$$

Therefore, the total electric field due to both electric and magnetic current sources is given by

$$\bar{E}(\bar{R}) = - \frac{jkZ_o}{4\pi} \frac{e^{-jkR}}{R} \bar{U} \quad ,$$

where the vector far field amplitude

$$(A20)\quad \bar{U} = -\int_{\text{source}} e^{jk\bar{R}'\cdot\hat{R}}\,\hat{R}\times(\hat{R}\times d\bar{p}_e(\bar{R}') + Y_o\,\hat{R}\times d\bar{p}_m(\bar{R}'))$$

In the case of an aperture lying in the xy-plane the equivalent surface current sources are given by

$$(A21)\qquad \bar{J}_s = \hat{z}\times\bar{H}^a \text{ and } \bar{K}_s = \bar{E}^a\times\hat{z}$$

where $\bar{E}^a$ and $\bar{H}^a$ are the aperture fields. If the source point is described in cylindrical coordinates $(\rho',0,\varphi')$ and the field point by spherical coordinates (R,θ,φ),

$$(A22)\qquad \bar{R}'\cdot\hat{R} = \rho'\sin\theta\cos(\varphi-\varphi')\quad .$$

REFERENCES

1. Jasik, H. and Bresler, A.D., "A Low Noise Feed System for Large Parabolic Antennas," in Electromagnetic Theory and Antennas (Proc. Symp. held at Copenhagen, Denmark, June, 1962) Ed: E.C. Jordan, New York: McMillan Co. (Pergamon Press Book), 1963, pp. 1167-1171.

2. Einstein, H.B. and Warner, H.B., "Mathematical Evaluation of Radio Frequency Hazards to Resistive Devices," IEEE Trans. Vol. EMC-7, No. 3, pp. 287-296 (1965).

3. Keller, H.B., "Diffraction by an Aperture," J. Appl. Phys., Vol. 28, No. 6, pp. 426-444 (1957).

4. Silver, S., Microwave Antenna Theory and Design, New York: Dover Publications, Inc., 1965, p. 158.

5. Silver, Opt. Cit., Chapters 5, 6, 12.

6. Fradin, A.Z., Microwave Antennas (Trans. from Russian) New York: Pergamon Press, 1961, Chapter 7.

7. Tartakovskii, L.B., "Side Radiation from Ideal Paraboloid with Circular Aperture," Radio Engineering and Electronics, Vol. 4, No. 6, pp. 14-28 (1959).

8. Silver, Op. Cit., p. 144.

9. Schouten, J.P. and Beukelman, B.J., "On the Radiation Pattern of a Paraboloid of Revolution," Appl. Sci. Res. (B), Vol. 4, pp. 137-150 (1954).

10. Afifi, M.S., "Radiation from Paraboloid of Revolution," in Electromagnetic Wave Theory-Part 2 (Proc. Symp. held at Delft, The Netherlands, September, 1965) Ed: J. Brown, New York: Pergamon Press, 1967, pp. 669-687.

11. Kinber, B.E., "Lateral Radiation of Parabolic Antennas," Radio Engineering and Electronics, Vol. 6, No. 4, pp. 481-492 (1961).

12. Lysher, L.J., "A Study of the Near-Field Behind a Parabolic Antenna," M.S. Thesis, The Ohio State University, Columbus, Ohio, 1962.

13. Peters, L., Jr., Notes on "Reduction of Radio Frequency Interference through Antenna Design".

14. Peters, L., Jr., and Rudduck, R.C., "RFI Reduction by Control of Antenna Sidelobes," IEEE Trans., Vol. EMC-6, pp. 1-11 (1964).

15. Peters, L., Jr., and Kilcoyne, T.E., "Radiating Mechanisms in a Reflector Antenna System," IEEE Trans., Vol. EMC-7, pp. 368-374 (1965).

16. Rusch, W.V.T., "Edge Diffraction from Truncated Paraboloids and Hyperboloids," Jet Propulsion Laboratory Technical Report 32-1113, California Institute of Technology, Pasadena, California (June 1, 1967).

17. Kouyoumjian, R.G., "Asymptotic High Frequency Methods," Proc. of the IEEE, Vol. 53, pp. 864-876 (1965).

18. Kouyoumjian, R.G., Unpublished Notes.

19. Braunbek, W., "Neue Naherungsmethode fur die Beugung am eben Schrim", Zeits fur Physik, Vol. 127, p. 381 (1950).

20. Keller, J.B., Lewis, R.M. and Seckler, B.D., "Diffraction by an Aperture II," J. Appl. Phys. Vol. 28, No. 5, pp. 570-579 (1957).

21. Jones, E.M.T., "Paraboloid Reflector and Hyperboloid Lens Antenna," Trans. I.R.E., Vol. AP-2, pp. 119-127 (1954).

22. Silver, Op. Cit., p. 344.

23. Sommerfeld, A., Optics, New York: Academic Press, 1964, pp. 247-272.

24. Pathak, P.H. and Kouyoumjian, R.G., "The Dyadic Diffraction Coefficient for a Perfectly-conducting Wedge," Paper to be published.

25. Ryan, C.E., "A Geometrical Theory of Diffraction Analysis of the Radar Cross Section of a Sectionally Continuous Second-Degree Surface of Revolution," Ph.D. Dissertation, The Ohio State University, Columbus, Ohio (1968).

UNCLASSIFIED

Security Classification

DOCUMENT CONTROL DATA - R&D

(Security classification of title, body of abstract and indexing annotation must be entered when the overall report is classified)

1. ORIGINATING ACTIVITY *(Corporate author)* ElectroScience Laboratory, Department of Electrical Engineering, The Ohio State University Research Foundation, Columbus, Ohio 43212	2a. REPORT SECURITY CLASSIFICATION: Unclassified 2b. GROUP

3. REPORT TITLE

THE WIDE ANGLE SIDE LOBES OF REFLECTOR ANTENNAS

4. DESCRIPTIVE NOTES *(Type of report and inclusive dates)*

Scientific Interim

5. AUTHOR(S) *(Last name, first name, initial)*

P.A.J. Ratnasiri
R.G. Kouyoumjian
P.H. Pathak

6. REPORT DATE	7a. TOTAL NO. OF PAGES	7b. NO. OF REFS
23 March 1970	57	25

8a. CONTRACT OR GRANT NO.	9a. ORIGINATOR'S REPORT NUMBER(S)
Contract AF 19(628)-5929 b. Project, Task, Work Unit Nos. 5635-02-01 c. DoD Element 61102F d. DoD Subelement 681305	ElectroScience Laboratory 2183-1 9b. OTHER REPORT NO(S) *(Any other numbers that may be assigned this report)* AFCRL-69-0413

10. AVAILABILITY/LIMITATION NOTICES

This document has been approved for public release and sale; its distribution is unlimited.

11. SUPPLEMENTARY NOTES	12. SPONSORING MILITARY ACTIVITY
TECH, OTHER	Air Force Cambridge Research Laboratories (CRD), L.G. Hanscom Field Bedford, Massachusetts 01730

13. ABSTRACT

The complete pattern of a parabolic reflector antenna has been calculated using the singly-diffracted rays of the geometrical theory of diffraction, with proper corrections for the forward and real axial directions. Excellent agreement with experimental patterns can be expected, if the aperture blockage is not significant.

The solution has the usual advantages of a solution based on the geometrical theory of diffraction, namely, it is obtained in the form of simple functions, its computation cost is low, it is directly related to the radiation mechanism of the antenna and so it can be readily used in the design problem, and it can be easily extended and modified as the need arises.

DD FORM 1 JAN 64 1473

UNCLASSIFIED

Security Classification

UNCLASSIFIED

Security Classification

14. KEY WORDS	LINK A		LINK B		LINK C	
	ROLE	WT	ROLE	WT	ROLE	WT
Reflector antenna Secondary pattern Diffraction Rear axial field Aperture field Waveguide feed Dipole feed Parabola Antenna measuring system						

INSTRUCTIONS

1. ORIGINATING ACTIVITY: Enter the name and address of the contractor, subcontractor, grantee, Department of Defense activity or other organization *(corporate author)* issuing the report.

2a. REPORT SECURITY CLASSIFICATION: Enter the overall security classification of the report. Indicate whether "Restricted Data" is included. Marking is to be in accordance with appropriate security regulations.

2b. GROUP: Automatic downgrading is specified in DoD Directive 5200.10 and Armed Forces Industrial Manual. Enter the group number. Also, when applicable, show that optional markings have been used for Group 3 and Group 4 as authorized.

3. REPORT TITLE: Enter the complete report title in all capital letters. Titles in all cases should be unclassified. If a meaningful title cannot be selected without classification, show title classification in all capitals in parenthesis immediately following the title.

4. DESCRIPTIVE NOTES: If appropriate, enter the type of report, e.g., interim, progress, summary, annual, or final. Give the inclusive dates when a specific reporting period is covered.

5. AUTHOR(S): Enter the name(s) of author(s) as shown on or in the report. Enter last name, first name, middle initial. If military, show rank and branch of service. The name of the principal author is an absolute minimum requirement.

6. REPORT DATE: Enter the date of the report as day, month, year, or month, year. If more than one date appears on the report, use date of publication.

7a. TOTAL NUMBER OF PAGES: The total page count should follow normal pagination procedures, i.e., enter the number of pages containing information.

7b. NUMBER OF REFERENCES: Enter the total number of references cited in the report.

8a. CONTRACT OR GRANT NUMBER: If appropriate, enter the applicable number of the contract or grant under which the report was written.

8b, 8c, & 8d. PROJECT NUMBER: Enter the appropriate military department identification, such as project number, subproject number, system numbers, task number, etc.

9a. ORIGINATOR'S REPORT NUMBER(S): Enter the official report number by which the document will be identified and controlled by the originating activity. This number must be unique to this report.

9b. OTHER REPORT NUMBER(S) If the report has been assigned any other report numbers *(either by the originator or by the sponsor)*, also enter this number(s).

10. AVAILABILITY/LIMITATION NOTICES: Enter any limitations on further dissemination of the report, other than those imposed by security classification, using standard statements such as:

(1) "Qualified requesters may obtain copies of this report from DDC."

(2) "Foreign announcement and dissemination of this report by DDC is not authorized."

(3) "U. S. Government agencies may obtain copies of this report directly from DDC. Other qualified DDC users shall request through

_____."

(4) "U. S. military agencies may obtain copies of this report directly from DDC. Other qualified users shall request through

_____."

(5) "All distribution of this report is controlled. Qualified DDC users shall request through

_____."

If the report has been furnished to the Office of Technical Services, Department of Commerce, for sale to the public, indicate this fact and enter the price, if known.

11. SUPPLEMENTARY NOTES: Use for additional explanatory notes.

12. SPONSORING MILITARY ACTIVITY: Enter the name of the departmental project office or laboratory sponsoring *(paying for)* the research and development. Include address.

13. ABSTRACT: Enter an abstract giving a brief and factual summary of the document indicative of the report, even though it may also appear elsewhere in the body of the technical report. If additional space is required, a continuation sheet shall be attached.

It is highly desirable that the abstract of classified reports be unclassified. Each paragraph of the abstract shall end with an indication of the military security classification of the information in the paragraph, represented as *(TS), (S), (C), or (U)*.

There is no limitation on the length of the abstract. However, the suggested length is from 150 to 225 words.

14. KEY WORDS: Key words are technically meaningful terms or short phrases that characterize a report and may be used as index entries for cataloging the report. Key words must be selected so that no security classification is required. Identifiers, such as equipment model designation, trade name, military project code name, geographic location, may be used as key words but will be followed by an indication of technical context. The assignment of links, rules, and weights is optional.

UNCLASSIFIED

Security Classification